Electron and proton transfer during conformational changes in

reaction centers reconstituted into liposomes

Hassan Akhavein

A Thesis

in

The Department

of

Physics

Presented in Partial Fulfillment of the Requirements
for the Degree of Master of Science (Physics) at
Concordia University
Montreal, Quebec, Canada

April 2011

Concordia University

School of Graduate Studies

This is to certify that the thesis prepared

By: Hassan Akhavein

Entitled: Electron and proton transfer during conformational changes in reaction centers reconstituted into liposomes

and submitted in partial fulfillment of the requirements for the degree of

Master of Science (Physics)

Complies with the regulations of the University and meets the accepted standards with

respect to originality and quality.

Signed by the final Examining Committee:

                                          _____Chair
                                          Dr. P. Vasilopoulos

                                          _____Examiner
                                          Dr. V. Zazubovitch

                                          _____Examiner
                                          Dr. A. Champagne

                                          _____Supervisor
                                          Dr. L. Kalman

Approved by   _____
                                    Chair of Department or Graduate Program Director

6/04/2011   _____
                                    Dean of Faculty

Abstract

Electron and proton transfer during conformational changes in reaction centers reconstituted into liposomes

Hassan Akhavein

Nature's photosynthetic energy conversion can be used as a potential model system for developing man made artificial solar energy converters. The conversion of solar energy to chemical energy takes place in a specialized pigment-protein complex called reaction center, which is emended in the photosynthetic membrane. Our goal was to store the energy generated by light induced charge separation across the membrane in the form of electric potential for a period of time much longer than the natural lifetime. For this, we systematically altered the environment of the reaction center protein by changing the head group charge of lipids that are making up the membrane. These environmental changes resulted in several order of magnitude differences in lifetime of the charge separated states. The different lifetimes of charge separated states were assigned to recombinations form various light-induced conformations. These lifetimes correlated with the observed kinetics of the proton release. The results are discussed in terms of the involvement of a slow proton pathway and a dielectric relaxation of the reaction center near the primary electron donor upon illumination. Studies of these conformational changes were leading us to store

energy in the form of electric potential energy caused by separated charges in a

hydrophobic environment for several hours.

Acknowledgement

Table of Contents

List of Figures

List of Tables and Schemes

Abbreviations

BRC	Bacterial reaction center
Rb.	*Rhodobacter*
Da	Dalton
$BChl_2$	Bacteriochlorophyll dimer
BChl	Bacteriochlorophyll monomer
Bpheo	Bacteriopheophytin
Q_A	Quinone A, primary electron acceptor of BRC
Q_B	Quinone B, secondary electron acceptor of BRC
P	Electron donor
I	Intermediate electron acceptors (Bpheo and BChl together)
Cyt c_2	Cytochrome c_2
CMC	Critical micelle concentration
Glu	Glutamic acid
Asp	Aspartic acid
Lys	Lysine
Arg	Arginine
Tyr	Tyrosine
EDTA	Ethylenediaminetetraacetic acid
LDAO	Lauryldimethylamine-oxide
TEN	Tris-HCl, EDTA, NaCl
TLE	Tris-HCl, LDAO, EDTA

NMWL   Nominal molecular weight limit

DOPC   1,2-dioleoyl-*sn*-glycero-3-phosphocholine

DOPE   1,2-dioleoyl-*sn*-glycero-3-phosphoethanolamine

DOTAP   1,2-dioleoyl-3-trimethylammonium-propane

MES   2-(*N*-morpholino)ethanesulfonic acid

Tris   Tris(hydroxymethyl)aminomethane

CHES   *N*-Cyclohexyl-2-aminoethanesulfonic acid

CAPS   *N*-cyclohexyl-3-aminopropanesulfonic acid

LFP   Laser flash photolysis

1. Introduction

1.1 Introduction to photosynthesis

Photosynthesis is a process that converts solar energy to chemical energy by using inorganic carbon dioxide and water into organic compounds, such as sugar. All the food we eat and all the fossil fuel we use are the products of photosynthetic activities in the recent or distant past. Photosynthesis is carried out by many different organisms, ranging from plants to bacteria. The best known form of photosynthesis is oxygenic photosynthesis carried out by plants and algae, as well as by cyanobacteria, which are responsible for a major part of photosynthesis in oceans. All these organisms convert carbon dioxide (CO_2) to organic material like carbohydrates in a rather complex set of reactions. Electrons for these reactions mainly come from water, which is then converted to oxygen and protons. Although plants are the most representative photosynthetic organisms, many other types of photosynthetic organisms exist. All photosynthetic bacteria other than cyanobacteria and their relatives cannot use water as the ultimate electron donor for thermodynamic reasons. Instead, they can use reduced compounds such as H_2S as donor. For example in the bacterial reaction center (BRC), exogenous cytochromes with much lower potentials act as secondary electron donors. The structural and functional similarities between the evolutionarily related PS II and the BRC but more simplicity in BRC make the latter a good model for studying biological energy conversion for years [1].

1.2 Structure of photosynthetic BRC from Rb.*sphaeroides*

The three-dimensional structure of BRC from *Rhodobacter (Rb.) sphaeroides* had been determined by X-ray diffraction method, which is elucidating the structure-function relationship with 2.8Å resolution [2, 3]. The BRC from photosynthetic bacteria is an integral membrane-protein complex, which contains three subunits (L- , M- and H-) with 5, 5 and 1 membrane-spanning α-helices, and 281, 307 and 260 amino acid residues, respectively with a total molar mass of ~100kDa (1Da (Dalton) = 1 g/mol))..
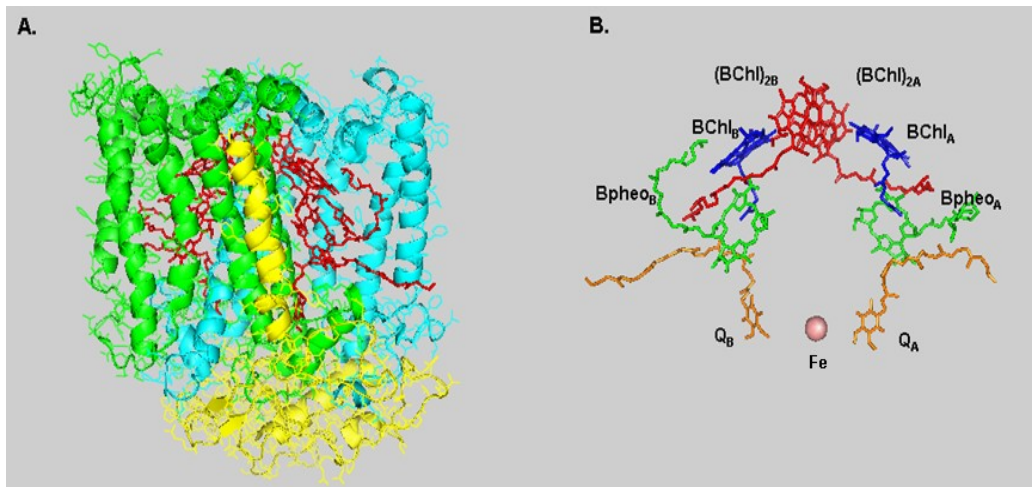
Figure 1.1 Structure of the BRC from *Rb. sphaeroides* A. The arrangement of protein subunits: L (Blue), M (Green), and H (Yellow). **B.** Nine cofactors of the BRC, which are aligned across the 2-fold symmetry axis passing vertically through the plane of paper from (BChl$_2$) to non-heme iron (Fe). Modified from Protein Data Bank PDB code: 4RCR [4]

Nine cofactors are found to be associated with   L- and M- subunits including one bacteriochlorophyll dimer BChl$_2$, two bacteriochlorophyll monomers (BChl$_A$ and BChl$_B$), two bacteriopheophytins (Bpheo$_A$ and Bpheo$_B$), two ubiquinones (Q$_A$ and

Q_B) and a non-heme iron. Cofactors are arranged in two branches, which are related to each other by and approximately 2-fold rotational symmetry axis (Figure 1.1).

1.3 Influence of protein isolation on the structure of the reaction center

Due to a large hydrophobic region of the BRC protein, it is not water-soluble and it has to be in amphiphilic environment to survive. In Nature, this membrane is made of combination of variety of natural phospholipids, phosphatidylcholine, phosphatidylethanolamin and other lipids, which are depending on the growth condition of the bacteria, such as oxygen level or temperature. The BRC has to be extracted from its natural membrane and has to be brought in to an artificial environment, such as detergent micelles or artificial membranes like liposomes. The isolation process allows better spectroscopic characterization, because the natural membrane, the antenna complexes, and cyt bc_1 will hamper the spectral properties of BRC. Detergents are inherently amphiphilic, made of hydrophilic head groups and hydrophobic alkyl chains. After isolation of BRC into detergent micelles, the hydrophobic chains of detergents will face toward the hydrophobic region of BRC and cover it like a belt to make it dispersible in a hydrophilic environment, like water (Figure 1.2). The thickness of the detergent belt was reported to be ~23 Å [10]. This thickness is about 5 Å thinner than the length of

transmembrane helices   detergent belt
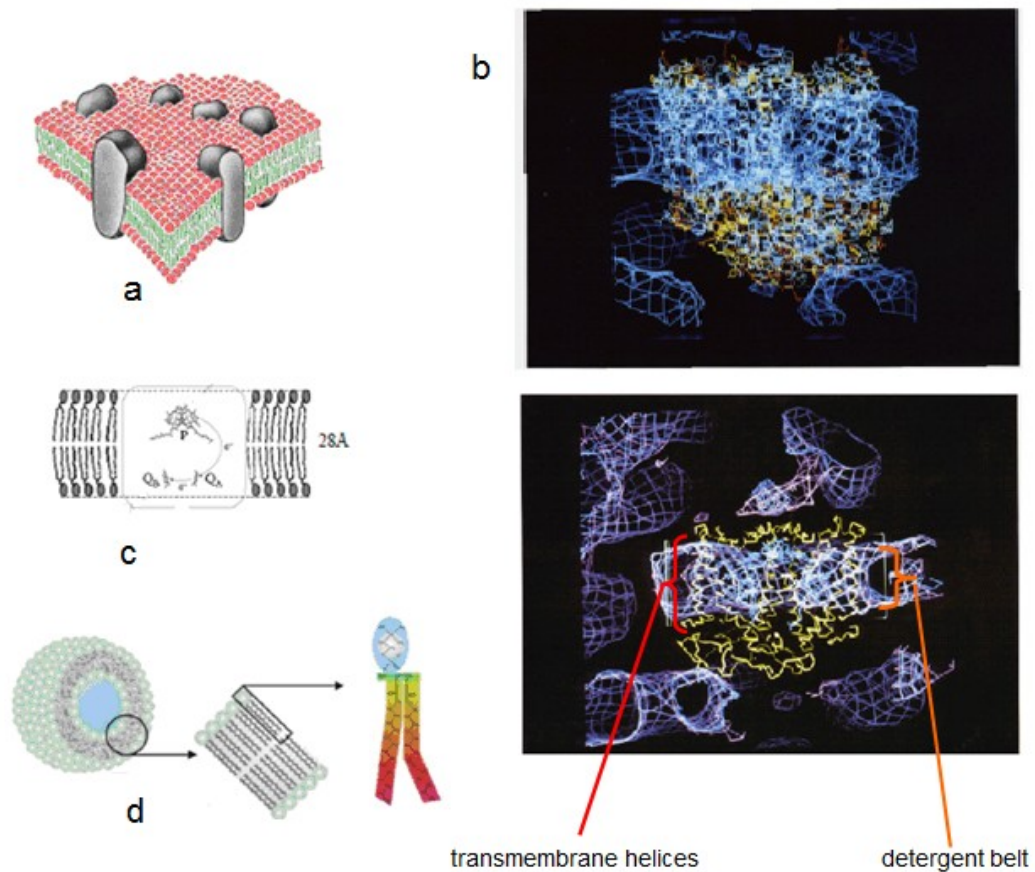
Figure 1.2 BRC in the natural membrane environment, in detergent micelles, and in liposomes. BRC from its natural membrane environment (a) can be isolated and incorporated into detergent micelles (b). These detergent micelles form a belt like structure around the hydrophobic environment of the BRC. The BRCs can be also incorporated into liposomes (c), which are formed from lipid bilayer (d). Figure was modified from [5].

the hydrophobic transmembrane helices. Concentration of detergent has to be higher than the CMC (critical micelle concentration), which is the limit for detergents to form micelles spontaneously [6]. After isolation of RC into detergent micelles, we can change the detergents to study BRC features in different environments. Even though the overwhelming majority of the

accumulated knowledge about the BRC has been gathered from samples that have been embedded in detergent micelles, as pointed out above this system is far from being the best representation of the natural system. Much better substitutes for the natural membranes are the liposomes. Liposomes are spontaneously forming a spherical bilayer structures from individual lipid molecules to minimize the solvent accessible surface. The lipids could have different chain lengths or even different head group net-charges at specific pH values, which can alter the function of BRC. The orientation of BRC center incorporated into detergent micelles and liposomes is slightly different (Figure 1.2). As mentioned earlier, the environment has significant influence on the characteristics of BRC, so by systematically changing the detergent and lipid environment of the BRC, we can tune the properties of the BRCs.

1.4 Electron transfer process in BRC

Light induces an electron transfer from the $BChl_2$ as an electron donor (P) to the secondary quinone Q_B through intermediate electron acceptors (I), which are $BChl_A$, $Bpheo_A$ and primary quinone Q_A.

Because of the huge difference in the free energy level between $BChl_A$ and $BChl_B$ due to the interaction of some natural lipids inside reaction center with cofactors and also lower local dielectric constant in B branch [7] the electron transfer is highly unidirectional via the A branch [8].

The free energy levels of the intermediate states makes the forward electron transfer steps more favourable because it is orders of magnitude faster than the

charge recombination reactions (Figure 1.3) For example , electron transfer from

Q_A^- to Q_B takes place in about 100 μs while charge recombination from $P^+Q_A^-$ to

PQ_A requires nearly 100ms.

The orders of magnitude faster forward reactions compared to the corresponding

back reactions in each step made this process one of the most effective cycle of

energy conversion. In the presence of an external electron donor, like cytochrome

c_2 (cyt c_2), which can reduce P^+, another electron can be transferred from P to Q_B
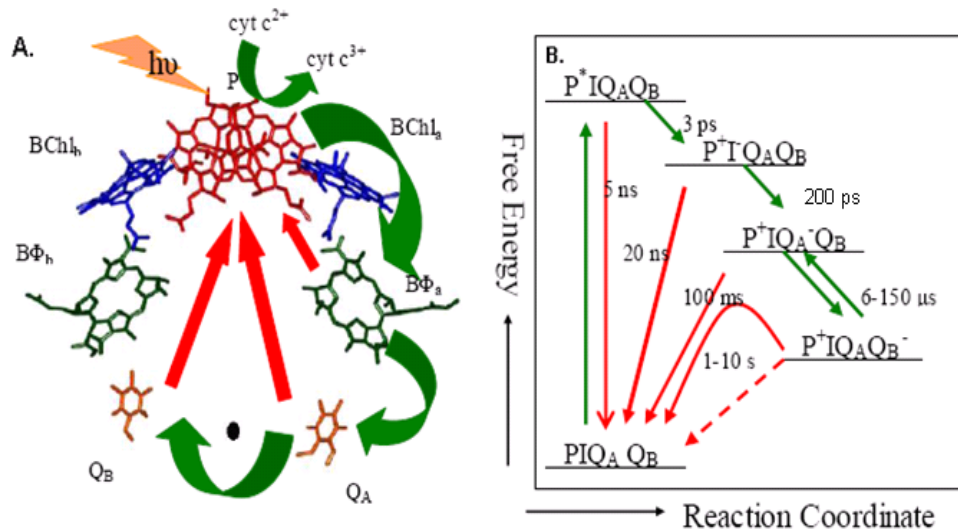
Figure 1.3 Light-induced electron transfer processes in photosynthetic bacterial reaction centers. A. The pathway of the light induced forward electron transfer steps are indicated by green arrows and the red arrows represent the charge recombination reactions. **B.** The energy levels of various redox states formed during the electron transfer process. As in panel A, the green arrows show the forward electron transfer steps while the red arrows show the charge recombination processes. P^+I^- represents intermediate charge separated states involving the dimer and the bacteriopheophytin.

but this time Q_B will accept two protons from the cytoplasmic side to become

quinol (Q_BH_2). Quinol is weakly bound to the protein and will shuttle the protons

and electrons across the membrane [9]. Despite of the 2-fold symmetry, Q_A and Q_B show different properties. Different redox potentials of these quinons make Q_A to perform as an electron donor to Q_B. The different redox properties come from amino acid residues near the ubiquinones and also from the nonheme iron, which is 2 Å closer to Q_B [10].

1.5 Photosynthetic electron transfer cycle in natural membrane

In natural membrane environment by transferring of two electrons from P and accepting two protons, the secondary quinon Q_B will form the quinol (Q_BH_2). Quinol is released from the protein to the membrane and will be replaced by another quinon from the pool. The released quinol will be oxidized by cytochrome bc_1 complex. This way there will be a quinon pool in the membrane, which can exchange quinons and quinols between cytochrome bc_1 and BRC (Figure 1.4). By oxidizing the quinol, cytochrome bc_1 can release protons to the periplasmic side, generating an electrochemical proton gradient. Meanwhile, electrons can be transferred from cytochrome bc_1 to BRC through the mobile electron carrier cyt c_2 to oxidize the primary donor (P) once again by the heme iron on the periplasmic side. Transmembrane proton gradient serves as the driving force for ATP synthesis [11].
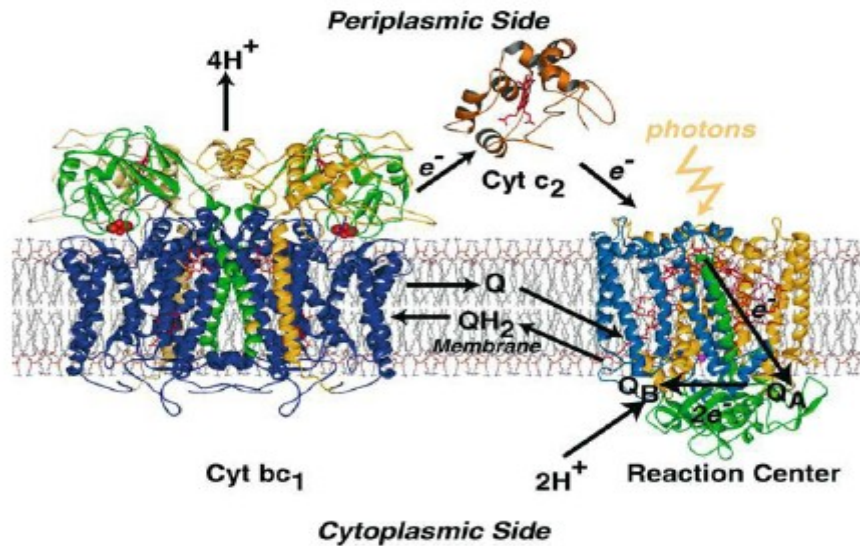
Figure 1.4 Schematic view of the cyclic electron transfer in the natural membrane of photosynthetic bacterium *Rb. sphaeroides*: Light induces a transfer of an electron from the $BChl_2$ of BRC through a series of electron acceptors to reduce the reversibly bound Q_B. Reduced quinone is being released from the BRC and being oxidized by the cytochrome bc_1 complex. The mobile electron carrier cyt c_2 accepts an electron from cytochrome bc_1 complex and migrates to the BRC to transfer an electron to re-reduce P^+. Each cycle pumps protons from cytroplasmic side into periplasmic side to form a proton gradient across the membrane.

1.6 Marcus theory of electron transfer

1.6.1 Franck-Condon principle applied to electron transfer

The principle that in any molecular system the transition from one energy state to another is so rapid that the nuclei of the atoms involved can be considered to be stationary during the transition is called Franck-Condon principle. Libby in his

paper in 1952 used Franck-Condon principle to explain why the electron transfer

between a pair of small cations in aqueous solution such as reaction

$$Fe^{2+} + Fe^{*3+} \rightarrow Fe^{3+} + Fe^{*2+} \qquad (1.6.1.1)$$
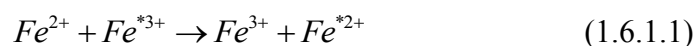
are relatively slow in comparison with larger ions like $Fe(CN)_6^{3-}$, $Fe(CN)_6^{4-}$ and

MnO_4^{2-} , MnO_4^{-}

Libby used a novel application of Franck-Condon principle, used extensively in

the field of spectroscopic measurements for the excitation of the molecular

electronic-vibrational quantum states) in calculating solvent energy barrier in

chemical reactions. By transferring an electron from one reactant to another, the

new system will be in a "wrong" environment of solvent molecules. This happens

because of configuration of many-body dipolar solvent molecules, which are not

in proper state for the new system. Electron transfer is very fast and during this

short time the nuclei cannot rearrange itself for new configuration. This is what is

often called as solvent energy barrier. On the other hand for larger ions such as

($Fe(CN)_6^{3-}$), because of the size of ions, influence of electric field by solvent is

pretty small and the new formed ions is less foreign to the solvent. Libby

explained the slow rate of electron transfer in (Fe^{2+}) and fast rate in ($Fe(CN)_6^{3-}$)

bye the height of energy barrier came from the solvent.

1.6.2 The Marcus Correction

In Libby's picture for electron transfer, the ions formed in the "wrong", higher

energy environment after the electron-transfer. So, it must be a source of energy,

which is responsible for the difference between energy of reactants and products

(and the solvent). We can refer to the absorption of light as the energy source for this process but what about the reactions, which occurring in dark? The energy is not conserved. So, there is something missing in Libby's picture. The question is how the reacting system behaves to satisfy both the Franck-Condon principle and the conservation of energy. Marcus claimed that there will be some fluctuation in various nuclear coordinates like orientation coordinates, which is most probable different in reactants and products. With such a fluctuation we can find some coordinates, which satisfy both Franck-Condon principle and energy conservation and allow the electron transfer to happen.

Assume that the total energy of the reactants and solvent molecules is U_r (Free energy of reactants). This energy depends on many coordinates of the system like position and orientation of the individual solvent molecules, their dipole moment, vibrational and rotational coordinates of reactants.
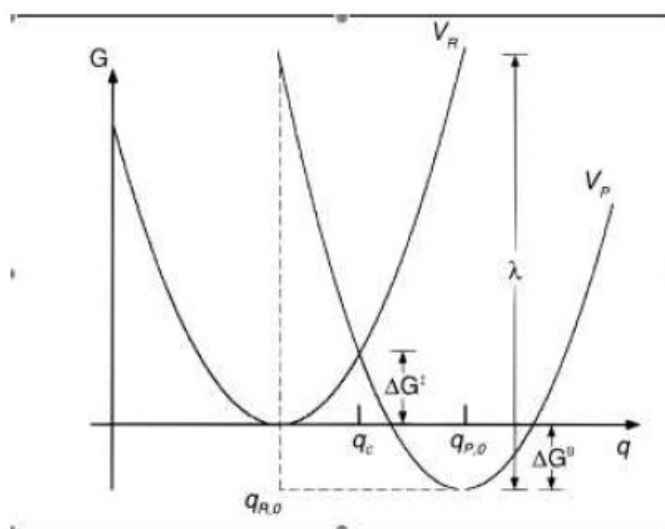
Figure 1.5 potential energy surfaces for reactant and products. Explanation is found in the text**.**

Before the reactions take place, there should be some fluctuation in these coordinates from their equilibria. For the system of N coordinates the intersection between reactants and products occurs on an N-1 dimensional surface (Figure 1.5). At the intersection between these two curves, the system is in a fix position and momenta so Franck-Condon principle is satisfied and V_r is equal to V_p (Free energy of products) , so the energy is conserved and the electron is permitted to transfer at that point even in the dark. By approximating the potential energy surfaces as parabolas, Marcus found an expression for the rate constant of such reactions by

$$k_{ET} = A\exp\left[\frac{-\Delta G^*}{K_B T}\right] = A\exp\left[\frac{(-\lambda + \Delta G^0)^2}{4\lambda K_B T}\right] \qquad (1.6.2.1)$$

Here ΔG^* is the free energy barrier, λ is reorganization energy and ΔG^0 is the Gibbs free energy. One of the interesting parts of this theory is that in some cases the increase of the difference between Gibbs free energies of the reactants and the products can decrease the rate constant of reaction, which have experimental evidence [12].

1.7 Stabilization of charge separated states by structural changes

The solvation of the newly created charges by individual electron transfer steps is often facilitated by secondary, compensating charge motions, which are coupled to conformational movements in the BRC chromophore-protein complex. Studies

of the slow conformational rearrangements upon illumination were inspired by the pioneering work of Kleinfeld and colleagues [13]. Many groups have followed their path in the past quarter of a century and provided new insights to the details of these changes [14-20]. Despite these extensive efforts, the exact molecular mechanisms of such conformational changes are still not clear. Most of the earlier conformational studies argued that the origin of the long-lived states upon continuous illumination must stem from conformational changes near the quinones [14, 16-19]. Very recently our research group reported light-induced electrochromic absorption changes that were attributed to a marked increase of the local dielectric constant near P [20]. The new conformations of the protein weaken the electrostatic interaction of P^+ with the protonatable residues of the BRC, causing light-induced proton release from periplasmic side of BRC. Other experimental evidence in our research group shows that the rate constant of charge recombination in the very longest lived charge separated state is limited by the rate of these protonation. The combination of light-induced optical spectroscopy, and protonational measurements are used here to identify the characteristics of the conformational states, in particular the energetics and protonational states when the BRC is incorporated into liposomes.

1.8 Light induced H$^+$ binding/unbinding in BRC

The proton uptake associated with electron transfer in BRC is the primary step of establishing transmembrane proton gradient [21]. There is protonation

equilibrium between light active BRC and aqueous bulk solution, which could be controlled by at least three processes, (a) formation of quinol [9], (b) energetic stabilization of redox states of BRC involving semiquinones [22, 23, 24] and (c) stabilization of light induced conformational changes [15].

1.8.1 Introduction to the acid base equilibria of the amino-acid side chains

There are 155 protonatable amino-acids in BRC, which have protonatable side chains that can uptake or release protons depending on the conditions. Let's assume we have an amino acid RA and its analytical concentration is [RA] in aqueous bulk solution. For the acid dissociation reaction $RH \leftrightarrow R^- + H^+$ equilibrium is described by its *pKa*, which is the negative logarithm of the acid dissociation constant defined as

$$-pK_a = \log(K_a) = \log(\frac{[H^+][R^-]}{[RH]}) \qquad (1.8.1.1)$$

Amino acid residues with protonatable side chains are able to make hydrogen bonds and change their charged states depending on the pH of environment. For example aspartic (Asp) and glutamic (Glu) acids have *pKa* values near 4 in aqueous solution, so they are expected to be protonated and negatively charged at pH 7. On the other hand, for example lysine (Lys), which has *pKa* around pH 10 is positively charged at pH 7. The solutional *pKa* values assume no interactions between the charges of these residues, since in aqueous solutions the individual amino acids can freely diffuse and avoid any unfavorable electrostatic interactions. Inside the protein, however, the amino acids are localized and cannot

13

escape from Coulomb and charge-dipole interactions. These interactions shift the *pKa-s* of the residues from the solution values [23, 24]. The extent and direction of the shift depends on the distance between the residue and another charge (on another amino acid) or dipole, and the value of the local dielectric constant [25]. A measure of the energy of single charges in a particular medium is its self energy E_s. This can be thought of as the energy of a charge in the absence of its counter-ion and thus defined by an expression similar to that of a charge-charge interaction [25].

$$E_s = \frac{q^2}{2DR_s} \qquad (1.8.1.2)$$

Here D is the dielectric constant of the medium and R_s is the effective molecular radius. The dependency on dielectric constant means that the self energy of an ion in hydrophobic environment (low dielectric constant) is much larger than what it is in water. This effect is reflected in a lower *pKa* for side chains of the basic amino acids and higher *pKa* for the acidic amino acids when they are buried into more hydrophobic environment [26]. We can treat the self energy as a perturbation to the dissociation constant by [25]

$$\Delta pK_a = \frac{\Delta E_s}{2.3k_BT} \qquad (1.8.1.3)$$

For example the *pKa* of Glu and Asp, which are acidic amino acids, may shift from 4 to 7 or even higher if they are buried into a protein environment of lower dielectric constant .

Another factor that shifts the *pKa* of residues is a presence of nearby charges, which can alter the energy of the residues. For example if we introduce a negative

charge near acidic amino acids placed in a hydrophobic environment, we can observe the increase of the *pKa* of these acidic residues, and an opposite direction of the shift is expected in the presence of a positive charge [23, 24]. Similarly, the *pKa* of a basic residue, like Lys or arginine (Arg) is expected to be shifted to a lower value if another positively charged residue or oxidized cofactor is placed nearby inside the protein.

1.8.2 Light induced H^+ binding of a single protonatable residue.

Figure 1.6 demonstrates the correlation between light-induced proton release and the *pKa* shift of a single protonatable residue. pH dependency of mole fraction of the protonated form (RH) is described by the Henderson-Hasselbalch equation.

$$f[RH] = \frac{1}{1+10^{pH-pKa}} \qquad (1.8.2.1)$$

The difference between two Henderson-Hasselbalch curves was used to explain stoichiometry of protonation of the amino acid residues in BRC, which is expressed by the following equation:

$$f(H) = A(\frac{1}{1+10^{(pH-pKa')}} - \frac{1}{1+10^{(pH-pKa)}}) \qquad (1.8.2.2)$$

where, *A* is the total number of available protonatable residues, *f(H)* is the fraction protonated, *pKa'* is the negative logarithm value of the proton dissociation constant in the presence of a positive charge and *pKa* is the negative logarithm value of the proton
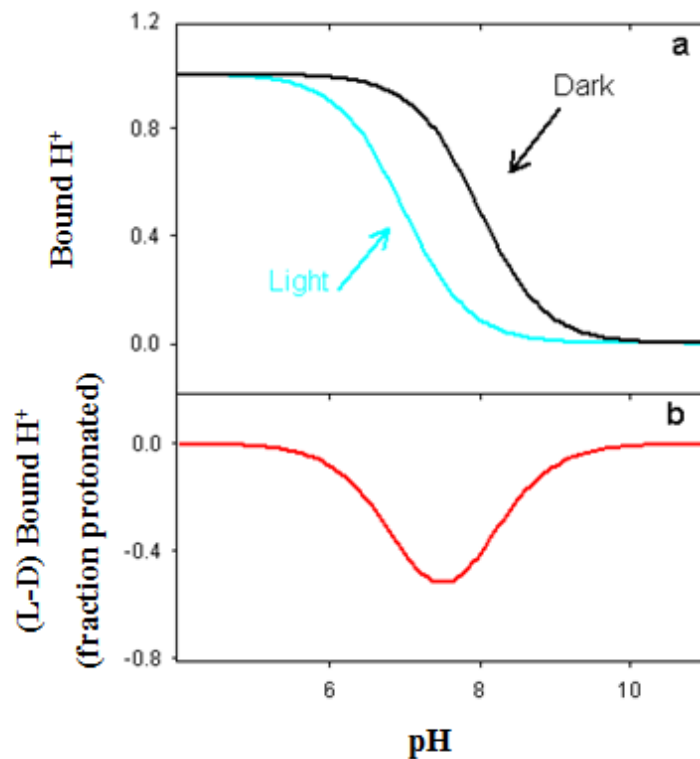
Figure 1.6 pH dependency of proton binding for a single protonatable residue (a) titration curve for single protonatable residue with a shift of the *pKa* by one pH unit in presence of a nearby charge (b) light-induced proton uptake determined as the difference between the two Henderson-Hasselbalch curves in panel a.

dissociation constant in the absence of a positively charge on $Bchl_2$. The presence of the light-induced positive charge on P will shift the *pKa* of residues near that region to lower pH (Figure 1.6 a). The difference between two Henderson-Hasselbalch curves (Figure 1.6 b) will represent the observable proton release caused by electron transfer.

1.8.3 Light-induced proton binding/unbinding due to energetic stabilization of redox states and stabilization trough conformational changes

As explained in (1.4), if a secondary electron donor like cyt c_2 is available, Q_B will accept two electrons from the primary donor in two subsequent electron transfer steps and two protons from the aqueous bulk solution will be delivered to form a fully reduced, fully protonated quinol (Q_BH_2). The stoichiometry of proton uptake by quinol formation is two protons per BRC.

Stabilization of semiquinones (Q_A^- and Q_B^-) in contrast to quinol formation, are followed by protonation and deprotonation of amino acid residues around these cofactors [23, 24]. These protonations are due to the presence of light-induced charges on cofactors and slight changes of local dielectric constant, which can result in a shift the *pKa* of these residues. Because this shift in *pKa* is caused by electrostatic interactions, the amount of shift is inversely proportional to the local dielectric constant of the surrounding protein as the medium. In BRCs, light-induced *pKa* shifts of about 0.5 to 1.5 pH units were observed earlier assuming four or five separated acid-base groups [23, 24].

These conclusions were drawn mainly from flash-induced proton binding measurements. There have been studies that suggested that the *pKa* shifts may be accompanied by conformational changes in the BRC [15, 20]. The relaxation of the BRC in response to the formation of the light-induced $P^+Q_A^-$ state is essentially completed in about 1 μs [27]. Long after the establishment of electrostatic, response in the protein, protonational reactions are still be

observable due to prolonged illumination. There are also quantitative disagreements between dielectric continuum calculations and experiments on the stoichiometry of proton binding/unbinding [28-32], which called for consideration of a third factor besides the proton transfer, such as conformational changes of the protein or displacement of internal water molecules [15, 20].

1.9 Optical spectrum of BRC

The BRC can be characterized by electronic absorption spectroscopy. Because the absorption bands of the individual chromophores are sensitive to changes in their nearby protein environment, both optical and Stark spectroscopies are useful tools for probing the changes of the local electrostatic properties upon excitation and relaxation. Stark spectroscopy had been applied successfully to monitor these changes not only in BRCs of purple bacteria but also in the photoactive yellow protein, where large photoinduced conformational changes were identified by detecting the band shifts of the chromophores [7].

The BChl as a planar molecule has two dipole moments directed in perpendicular directions and termed as Q_x and Q_y, which are along rings D to B and rings C to A, respectively (Figure 1.7). The absorption band corresponding to the Q_y transition of P has a peak at around 865 nm while for the BChl monomers are around 800 nm, and for Bpheo are around 760 nm. The absorption band for the Q_x transition of BChl and Bpheo have peaks at 600 nm and 540 nm, respectively.

The band at 400 nm is due to the porphyrins and at 280nm is coming from amino acids [33].
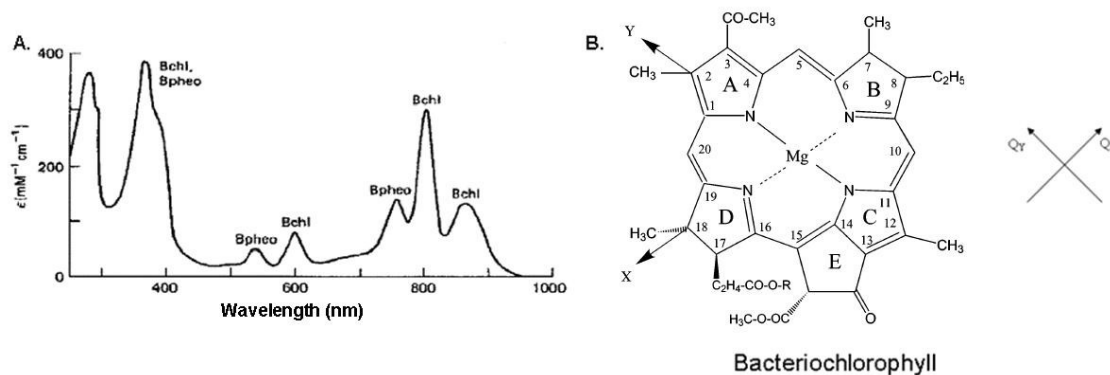
Figure 1.7 A: Absorption spectrum of the BRC Optical absorption spectrum of isolated RC with the absorption peaks at 865, 800, 760, 600, 540, 400 and 280nm. B: **Structure of bacteriochlorophyll molecule.** The bacteriochlorophyll molecule has two dipole moments along Q_X and Q_Y transition from ring D to B and from ring C to A respectively. R is a phytyl chain.

The spectroscopic characterization of the BRC detects the changes of these absorption bands induced by the absorption of the photon and the subsequent electron transfer. The bands can be bleached (absorbance decrease), shifted, or broadened in response to light. The former is due to a formation of a new species, whereas the latter two is due to the change of the polarizability and dipole moment of the chromophores, respectively. These changes can happen due to conformational changes near these cofactors or by introducing charges on $BChl_2$ and quinons by electron transfer upon illumination.

In our measurements, the near infrared region (700 -1000 nm) was used because not only the bacteriochlorophyll dimer (P) has a strong absorption band at ~865nm, but also the nearby bacteriochlorophyll monomers at ~800 nm. By

absorbing a photon by P, electron transfer takes place and when P has become oxidised, its absorption band will bleach. Bleaching of the P band is not the only sign of the electron transfer in the absorption spectrum. There are shifts and possible broadenings in the bands of the BChls and Bpheos (Figure 1.8).
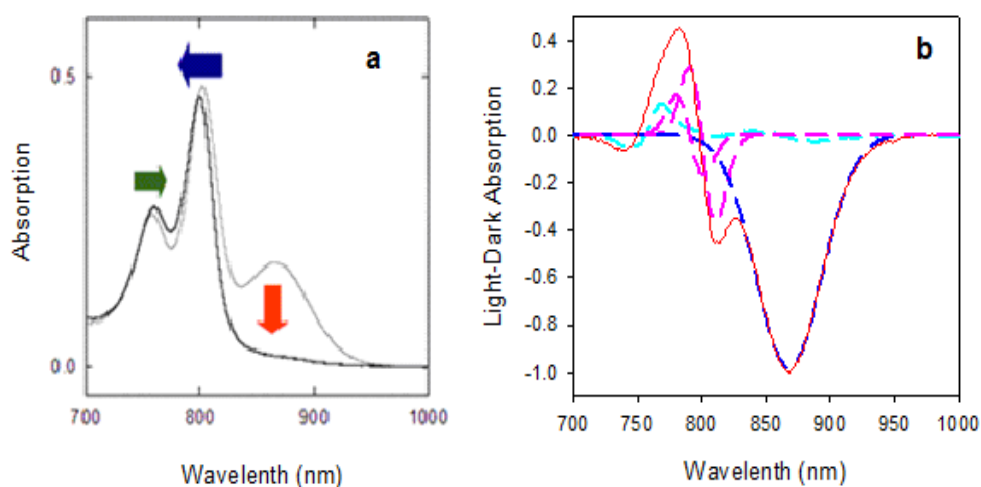
Figure 1.8 Near-Infrared light-minus-dark difference spectrum of BRC. A. The absolute spectrum of BRC in the dark is shown in gray. Upon illumination with intense light, electron transfer takes place from the P to Q_A resulting in the bleaching of the P band, a hypsochromic shift in the BChl monomer bands and a bathochromic shift in the Bpheo bands. The spectrum recorded under illumination is shown in black. **B.** Light-minus-dark difference spectrum (red trace) can be fit to the sum of Gaussians for P (blue dashed curve), BChl monomers (pink dashed curves) and Bpheos (cyan dashed curve) to determine the shifts in the band positions from dark adapted to light adapted states. In this sample, which is the BRC incorporated into DOPC liposomes. The BChl$_a$ had been shtifed from 805 nm to 796 nm and BChl$_b$ has been shifted from 794 nm to 788 nm.

The light-minus-dark difference optical spectra were analysed by assuming Gaussian curves for each absorption band and the widths and the peak positions were determined from the absolute (dark, recorded without saturating excitation)

20

spectra. The light-induced changes in the spectra were followed as the extent of bleaching and the shifts and broadenings of the absorption bands [16, 33].

1.10 Research perspective

The electron transfer in BRC is accompanied by translocation of protons and we are particularly interested in the coupling between these electron and proton transfer reactions. The first objective of the project is to explore the conformational changes caused by the light-induced electron and proton transfer reactions in BRC incorporated into various liposomes.

One of the precursors of the proton transfer is the electrostatic interaction between the light-introduced charge on the $BChl_2$ and the protonatable head groups of the amino acid side chains of the protein in the periplasmic side of BRC. The protonation/deprotonation processes of these residues electrostatically stabilize the charge pair and influence the electron transfer rate.

Since BRC is capable of separating the positive and negative charges in a medium with low dielectric constant, it could be a potential model to make man made artificial photosynthetic energy converter. The ultimate goal of this study is to utilize the BRC as a biocapacitor by systematically altering the membrane environment of the BRC protein involving the alteration of pH and the charge of the head groups (+1, 0, -2) of the lipids building up the membranes. With these systematic changes we could increase the lifetimes of charge separated states by 5 orders of magnitude.
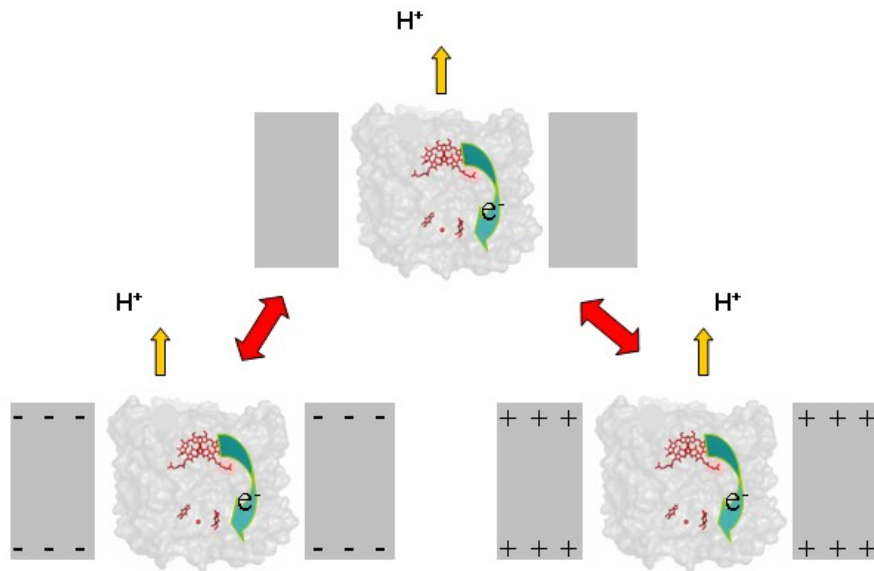
Figure 1.9 Altering the membrane environment of BRC. Head group charges of the membrane lipids were systematically altered. The gray shaded areas represent the lipid bilayers with different head group charges.

The novelty of this study lies in the fact that the electrostatic interactions and only few of the conformational changes had only been explored in detergent isolated BRCs but not in lipid environments, which represent better model systems to mimic the natural membranes than detergent micelles.

2. Materials and methods

2.1 Growth of *Rb.sphaeroides* bacterium

Cultures from carotenoidless mutant (R-26) of *Rb. sphaeroides* were grown under nonaerobic conditions and the BRCs were isolated and purified for all experiments according to [34]. The procedure involves preparation of growth media, sterilization, inoculation and growing the bacteria in presence of light. Growth media contains, 4 g casamino acid, 4 mL of growth factor, 40 mL of potassium succinate, 25 mL of ammonium sulphate, 80 mL of concentrated base and 80 mL of phosphate buffer. The final volume of the solution has to be adjusted to 4 L by distilled water.

Growth factor contains 2 mg of biotin, 50 mg of sodium bicarbonate, 50 mg of thiamine-hydrochloride, 100 mg of nicotinic acid and 100 mg of p-amino benzoic acid. For dissolving any ingredients, the solution was boiled and the volume was adjusted to 100 mL. Final solution was autoclaved in three small vessels.

The potassium succinate solution (20% m/V) was prepared by dissolving 200 g of succinic acid in 250 mL water, succinate did not dissolve completely. In separate beaker 200 g of potassium hydroxide was dissolved in 250 mL distilled water and cooled in an ice bath. In the ice bath potassium hydroxide was added into the beaker containing succinic acid slowly and the final volume was adjusted to 1 L and the pH was adjusted to 7 by concentrated HCl.

The ammonium sulfate solution (10% m/V) was prepared by pouring 50 g of ammonium sulfate into 500 mL of water and adjusting the pH to 7.

Concentrated base contains 2 g ethylenediaminetetraacetic acid (EDTA) , 5 g ferrous iron sulphate-heptaphydrate, 11 g zinc sulphate-heptaphydrate , 400 mg cupric sulphate-heptaphydrate ,370 mg cobalt chloride-hexahydrate, 120 mg boric acid and 1.5 mL 6 N sulphuric acid dissolved in distilled water . The final volume was adjusted to 1 L and final pH was adjusted to 7 by potassium hydroxide solution.

The 1 M phosphate buffer stock solution was prepared by dissolving 274 g dibasic potassium phosphate in 1200 mL water and 136 g monobasic potassium phosphate in 800 mL water in separate a beaker. Final solution was made by combining these two solutions and adjusting the volume to 2 L and the pH to 7.

All solutions were stored in 4° C.

The growth media was sterilized in an autoclave (type SV-120) for an hour to remove all the contamination. Inoculation with bacteria was done beside a Bunsen burner to avoid the contamination of the cells with other bacteria after cooling down the growth media to room temperature. Inoculated media was kept in dark from 3 to 6 hours for consuming all the oxygen remained dissolved in the media by respiration. Bacteria were grown under anaerobic conditions in the presence of light for 2 to 3 days and finally the grown bacteria was harvested by centrifugation at 4° C at 7000 times of acceleration of gravity (7000 g) using Beckman J2-HS centrifuge with JA-10 rotor. All cells were collected and stored at -20° C.

2.2 Purification of BRC

The BRCs were isolated and purified according to method described earlier [34]. 100 g of collected cells were stirred in 200 mL distilled water with 2 mL of 1 M Tris buffer for about one hour to obtain a homogenous solution. Then 2 mL of EDTA and 1.25 g of sodium chloride and 1.7 mL of lauryldimethylamine-oxide (LDAO) detergent was added and the solution was sonicated for 40 minutes with 10 s intervals in an ice bath (for avoiding excessive heat) to break the cells using an ultrasonic processor (Mandel Scientific company, Model XL2020, Farmingdale, NY ,USA). The final volume of the solution was adjusted to 210 mL and centrifuged in 8 tubes at 200000 g at 4^oC for 2 hours using an ultracentrifuge (Beckman, Optima XL-100K, Fullerton, California, USA) with a titanium (Ti-70, certified up to 70 000 rpm) rotor. The pellets were resuspended in 205 mL TEN (15mM **T**ris-HCl, 1 mM **E**DTA and 0.1 M **N**aCl), then 4.66 mL LDAO was added and the solution was stirred in dark for 10 minutes at room temperature. Solution was centrifuged with the same parameters as mentioned above with ultracentrifuge. Pellets, which contain cell membranes were discarded and the crude BRCs were collected from the supernatants. Corresponding to the amount of collected supernatants, ammonium sulfate and LDAO (for 220 mL supernatant, 72 g ammonium sulfate and 7.3 mL of 30% LDAO) were added to the supernatant solution and stirred for 15 mins at 26 ^{0}C. The solution was centrifuged at 10000 g at 4^oC for 15 mins using Beckman J2-HS centrifuge with JA-17 rotor. Crude BRCs were resuspended in TEN and dialysed overnight to

remove ammonium sulfate in $TL^{0.1}E$ (15 mM **T**ris-HCl, 0.1% **L**DAO, and 1 mM **E**DTA).

Ion exchange chromatography was used for further purification of BRCs. The Toyopearl GigaCap Q-650M column was pre-equilibriumed with $TL^{0.1}E$, then the protein was loaded into the column to bind to the column material. By loading $TL^{0.1}E$ and applying a salt gradient from 0.03 to 0.25 M using NaCl, the BRC protein was isolated and separated from any other pigments. The purity of protein was checked by taking the ratio of absorption spectra at 280 and 800 nm. This ratio was kept below 1.5 for all purifications (the purest sample has a ratio of 1.2 from these wavelengths). For the pure BRC the absorption band for P, Bchl monomers and Bpheo at 865, 800 and 760 nm has to have a ratio of 1:2:1 according to the structural stoichiometry. The BRC was dialysed overnight in $TL^{0.025}E$ (15 mM **T**ris-HCl, 0.025% **L**DAO, and 1 mM **E**DTA) to remove any residual salt. The dialysis was done at 4^oC in the dark. For all the dialysis, dialysing membranes were used with a **m**olecular **w**eight **c**ut **o**ff (MWCO) values of 12-14 kDa .

The BRCs were further concentrated by ultrafiltration using Millipore membranes (**n**ominal **m**olecular **w**eight **l**imit (NMWL) of 30kDa) by applying nitrogen pressure. Final concentration was determined from absorption band of Bchl at 800 nm, which has an excitation coefficient of $288\, mM^{-1}cm^{-1}$. Purified protein was stored in -80^oC in dark. All the chemicals were ordered from Sigma-Aldrich.

2.3 Liposome preparation

Reconstitution of BRCs from detergent micelles into proteoliposomes was done following the standard procedure [35]. 4 mg of phospholipids were dissolved in 200 μL chloroform in a 1.5 mL Eppendorf tube and the chloroform was evaporated with continuous nitrogen stream to form a thin layer of phospholipids inside the tube. The film can be stored in -20° C for a month. The lipid film was dissolved in 0.5 mL of 4% sodium cholate and sonicated for 45 mins with 10 s intervals using the same ultrasonic processor that was used for breaking the cells to form lipid-detergent mixed micelles. Then 100 μL BRCs with 25 μM concentration were added to the solution and were vortexed at 2500 rpm for 2 mins to form detergent-lipid-protein mixed micelles. The final dispersion was loaded into 15 cm long Sephadex G-50 gel filtration column. The column was pre-equilibrated and packed with a buffer. The identity of the buffer was dependent on the desired pH of the experiment. Lipid-protein mixed micelles, (which rearranged into protoliposomes and separated from detergent during elution) were collected at the end. Incorporation of BRCs into liposomes was checked by light-scattering measurements from the absorption spectra of BRCs. The fractions with the highest scattering were collected.

All the liposomes used in the present work were formed from phosphotidylcholines with the same fatty acid chain lengths of 18 carbons and the head group charges were systematically varied. All lipids were ordered from

Avanti Polar Lipids (Alabaster, Alabama, U.S.A.) and were used without further purification ($>99\%$).

The following three lipids were used in our measurements.

1,2-dioleoyl-*sn*-glycero-3-phosphocholine (DOPC)

1,2-dioleoyl-*sn*-glycero-3-phosphoethanolamine-N-(glutaryl) (DOPEG)

1,2-dioleoyl-3-trimethylammonium-propane (DOTAP)

2.4 Buffer preparation

Different buffers were used for different pH dependency measurements. Buffers were prepared from distilled water with concentration of 15 mM of respective buffer and 15 mM NaCl. Buffers, which were used for different pH, were 2-(*N*-morpholino)ethanesulfonic acid (MES) for pH 5.5 and 6, phosphate buffer for pH 7, tris(hydroxymethyl)aminomethane (Tris) for pH 8, *N*-Cyclohexyl-2-aminoethanesulfonic acid (CHES) for pH 9 and *N*-cyclohexyl-3-aminopropanesulfonic acid (CAPS) for pH 10.

2.5 Laser flash photolysis (LFP)

A laser flash photolysis unit (LFP-112 from Luzchem Research, Inc, Ottawa, Ontario, Canada) was used for measuring the charge recombination in BRCs. The BRC was excited at 532 nm with a 5 ns saturating laser pulse generated by a Nd:YAG laser (Model MINILITE II from Continuum, Santa Clara, California,

U.S.A.) and data were collected by monitoring the absorption changes at 865 nm on a digital storage oscilloscope (Tektronix TDS-2012, Tektronix, Beaverton, Oregon, U.S.A.) in DC coupled mode (Figure 2.1). On the first step, shutter 2 opens the way for the beam of Xe-lamp to path through the sample and absorption will record by the detector from the monochromator and will send to the computer through the digitizer. Then shutter 1 will let a laser flash of 5ns excite the sample and the absorption changes will monitor in time scale of about 200 ms by the same procedure.
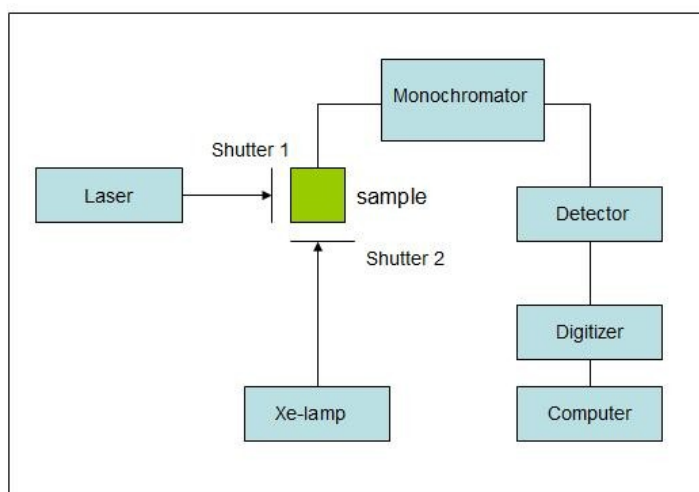
Figure 2.1 Schematic diagram for the setup of the LFP

In all the measurements BRCs with concentrations of at least 4 μM were used and 20 traces with manual laser trigger with 5 s intervals were averaged to improve the signal to noise ratio. The recorded traces were analysed using Sigma-Plot software using non linear Marquardt algorithm.

2.6 Steady state absorption spectroscopy

Measurements for charge recombination and conformational changes in BRCs were performed with a two beam spectrophotometer (Cary 5000 UV-Vis-NIR, Varian, Mulgrave, Victoria, Australia). An external light source (Oriel, 6129, Stamford, CONN, USA) tungsten lamp with output power range of 40 to 280 W for illumination of BRC was connected to the spectrophotometer via a fibre optic. Light induced states of BRC were generated by continuous illumination with different light intensities, which was controlled by the power supply (AMETEK, Sorensen, DCS33-33E, San Diego, CA, USA). All the measurements were performed in 3 mL quartz cuvette with following parameters for the spectrophotometer: range: 700-1000 nm; time averaging: 0.033 s; data interval: 0.5 nm.

Kinetic traces were recorded in kinetics mode at the wavelength corresponding to the peak of the absorption band of P.

2.7 Light-induced proton measurements

After purification, the BRCs showed little secondary quinon activity. 100 μM terbutryn was added as an inhibitor of interquinone electron transfer to block the electron transfer beyond Q_A. The sample was dialysed using membranes with MWCO of 12-14 kDa in dialysing bath containing 100mM NaCl and 0.05% Triton X-100 in order to remove EDTA, adjust the ionic strength to 100mM, and

replace the ionic detergent (LDAO) with a non-ionic detergent (Triton X-100). After 48 hours dialysis at 4° C with 3 times changing of dialysis medium, the concentration of Tris buffer was reduced to less than 1 μM, which gave negligible buffering capacity even at pH 8. Liposomes prepared with the same procedure as described in section 2.3 but here the sample were loaded without any buffer and with 100 mM NaCl into the column. Samples were collected from 3 to 4 separate columns and were merged to bring the final concentration of BRCs to at least 4 μM in order to have a good signal to noise ratio.

Light induced proton uptake/release of BRC was measured by a pH electrode (Thermo, Orion model 8103BNUWP, Beverly, MA, USA) and pH meter (Orion model 920A+) (Figure 2.2).
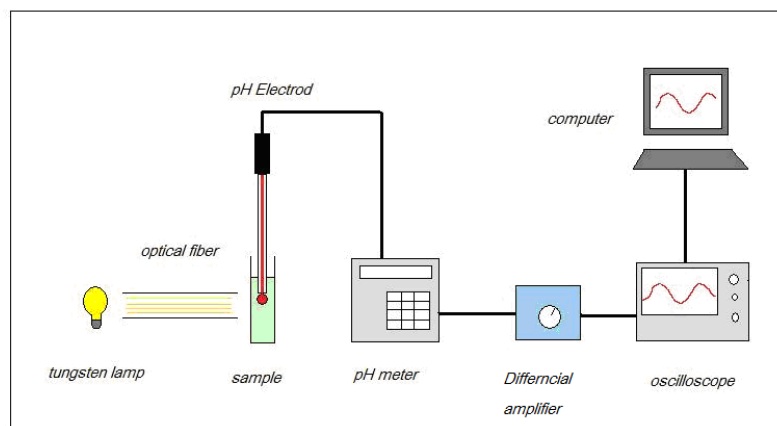
Figure 2.2 Block diagram of proton measurement setup. Data was transferred through the network to a computer for analysis.

The pH of the sample was recorded prior to the illumination. During and after illumination, the pH changes of the sample was monitored as a function of time by the pH meter and sent to the computer through the differential amplifier and the oscilloscope for analysis.

The stoichiometry of proton unbinding was determined by titrating the sample with known amount of H^+ using HCl. 10 mM HCl and 10mM NaOH were used for titrations. All the chemicals were stored under nitrogen pressure after preparation to avoid the absorption of carbon dioxide, which can act as a weak buffer in the carbonic acid $\Leftrightarrow$ bicarbonate equilibrium.

2.8 Data analysis

2.8.1 Analysis of the kinetic traces

Exponential fitting was used for analysing the various components of the kinetics of charge recombination in LFP and steady state absorption measurement. Decomposition of different components was analysed according to following equation:

$$A(t) = Be^{-k_1 t} + Ce^{-k_2 t} + De^{-k_3 t} \qquad (2.8.1.1)$$

where, A is the total signal amplitude as a function of time, B, C, and D are the amplitudes of each decaying component, t is time, k_1, k_2, and k_3 are the rate constants of the kinetic components. The lifetime (τ) of each component was calculated by the following equation

$$\tau = \frac{1}{k} \qquad\qquad (2.8.1.2)$$

2.8.2 Spectral contribution from different cofactors

Ground state spectrum was fitted by sum of Gaussians for P, Bchl monomers, and Bpheos by the following equation:

$$G = Ae^{-0.5 \times (\frac{x-x_0}{b})^2} \qquad\qquad (2.7.2.1)$$

Where, G is the absorbance at any given wavelength, A is the maximum value of the absorbance, x is the wavelength, x_0 is the peak position in the wavelength scale and b is the bandwidth at half maxim.

3. Results

3.1 Illumination time dependency of charge separated states in BRC incorporated into liposomes.

3.1.1 Spectral features of conformationally altered charge separated states upon prolonged illumination

Light-Dark optical difference spectra were recorded during and after prolonged illumination of BRC. Representative spectra are shown in (Figure 3.1). These spectra, which are the difference between the absorption in the particular charge separated states of BRC minus the absorption spectrum of BRC before any excitation were decomposed into following contributions. A bleaching in the $BChl_2$ band at 865 nm, shifts in the two BChl monomers at 794 and 805 nm and in Bpheo bands at 760 nm. The absorption band at 865 nm reveals the population of redox states after and during the illumination. Because the excitation was subsaturating, about 30% of BRC excited at the beginning of the illumination, the further decrease in the absorption band of $BChl_2$ can be interpreted as arising from another light-induced state being formed with longer lifetime. 30 minutes after turn off the illumination, the spectra almost recovered in case of dimer band position. But small electrochromic shifts in monomer didn't recover even after several hours. Spectra were recorded from 1 μM of BRC from R-26 mutant incorporated into liposomes forms from DOPC lipids at pH 8 with 15mM NaCl and 100 μM terbutryn upon 5 min of illumination. The tungsten lamp (80 W) was used as illumination source.
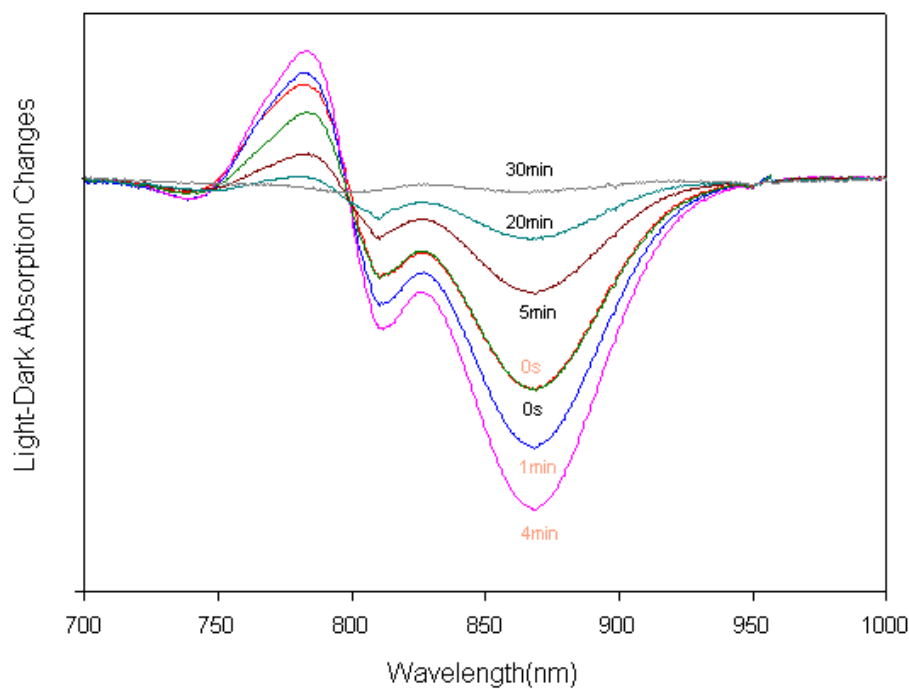
Figure 3.1 Near-infrared light-minus-dark optical difference spectra. Steady state absorption difference spectra reveal the features from the oxidized $BChl_2$ at 865 nm, the hypsochromic shift in BChl and bathochromic shift in Bpheo bands. The spectra were recorded at various illumination times up to 5 minutes and during the recovery in the dark after the illumination was turned off. The color code and numbers are representing the time during (Orange) and after (Back) illumination. Conditions: 0.5 μM of BRC in DOPC liposomes at pH 8 with 15mM NaCl and 100 μM terbutryn and 15mM Tris buffer. The tungsten lamp (80 W) was used as illumination source.

Comparison of the spectra reveals different electrochromic absorption changes in BChl monomers in different illumination time with the same population of P^+, which should indicate the altered conformation due to the prolonged illumination. (Figure 3.2) Analysis of these spectra revealed that there is an immediate shift prompt after illumination in $BChl_B$ band from 805 to 796 nm. Further illumination

caused complete relaxation to 799 nm. The BChl$_A$ shows similar behaviour. There is a blue shift from 794 nm to 788 nm immediately after illumination starts and a red shift to 789 nm after 4 minutes of illumination. The band width of the BChl$_a$ and BChl$_b$ were 10.7 nm and 10.1 nm respectively with the amplitude of 0.64 when the dimer band was normalized to one. These band width did not change significantly upon prolonged illumination. The error in the band position has been estimated to be less than 1 nm in fittings.
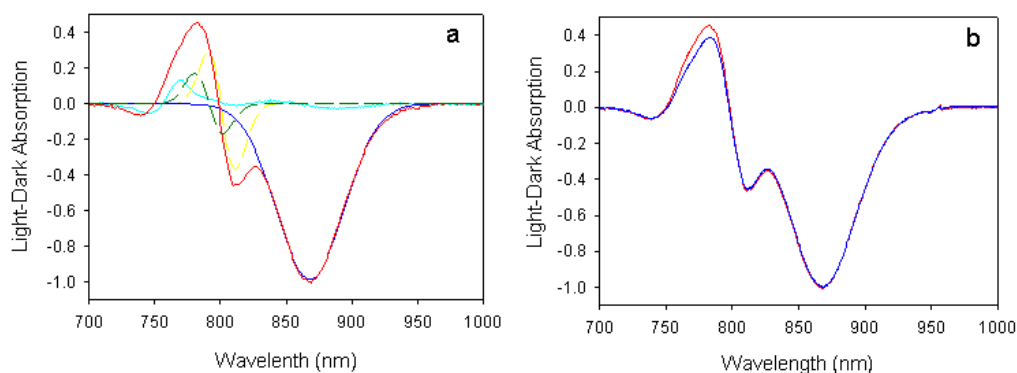
Figure 3.2 Light-Dark absorption spectra of BRC incorporated into DOPC. The spectrum was measured prompt after starting illumination (a) and compared with the spectra collected after 4 minutes of illumination (b). For better comparison the normalized spectra are shown. In panel (a), decomposition of these spectra, which was done by Gaussian curves, shows a bleaching in dimer band position (blue curve) and blue shifts in BChl monomers (dashed green and dashed yellow lines). Cyan curve, which is Q^-/Q spectra, was subtracted from the spectra prior to any fitting. Analysis represents that initial illumination makes a blue shift in the BChl monomers bands and prolonged illumination reverses these shifts. The values of the shifts are described in the text. Condition as (Figure 3.1)

In summary, in all the BRCs reconstituted into different liposomes in various pHs, initial illumination causes blue shift in the BChl monomer bands and prolonged

illumination reverses these shifts. These later changes lead to the longer lifetimes of the same charge separated state in different conformations. These absorption changes were in agreement with measurements in detergents that had been done by my colleagues.

3.1.2 Kinetic analysis of charge separated states in various illumination times.

To study the different conformations of the charge separated states, kinetics of the absorption changes were recorded as a function of time at the peak position of the Q_y band of the BChl$_2$ molecule centered at 865 nm. These kinetic traces were recorded at various illumination times from 5 ns transient laser flash excitation to several minutes of continuous illumination using tungsten lamp.

3.1.2.1 Recovery of the charge separated state after single flash excitation

Kinetic trace of $P^+Q_A^- \rightarrow P\,Q_A$ charge recombination was recorded in BRC incorporated into DOPC liposome at pH 8 after 5 ns laser flash excitation at 532 nm (Figure 3.3). The kinetic trace could be well characterized with a single exponential fit, which will indicate that upon flash excitation, the recovery of P^+ is a unidirectional process. Absorption changes were monitored at 865 nm and lifetime of the recovery was measured to be 95 ± 5 ms. This lifetime has been reported to be ~100 ms in detergent [37].

37
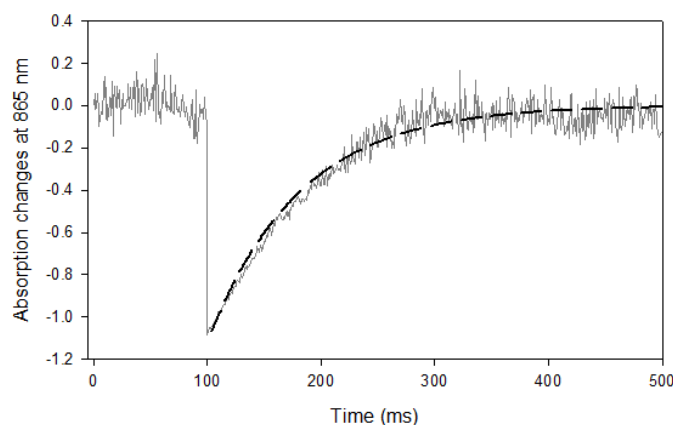
Figure 3.3 Kinetic trace of flash induced $P^+Q_A^- \rightarrow P \; Q_A$ charge recombination recorded in DOPC at pH 8. A 5ns laser flash was given and the recovery kinetic trace was analysed using a single exponential fit. The fitting resulted lifetime of 95 ± 5 ms. Conditions: 4 μM BRC incorporated into liposomes formed from DOPC at pH 8 with 15mM Nacl and 15mM Tris buffer. In order to block the electron transfer from Q_A to Q_B , 100 μM terbutryn was added.

3.1.2.2 Recovery of the conformationally altered charge separated state upon prolonged illumination

Absorption changes upon prolonged illumination were monitored at the dimer band position at 865 nm. 1 μM of BRC from R-26 mutant incorporated into liposomes formed from DOPC lipids at pH 8 was illuminated by a tungsten lamp (80 W) and a series of the kinetic traces were recorded at the dimer band position by varying illumination time from 1 to 15 minutes (Figure 3.4).

Immediately after the illumination was turned on, a fast kinetic phase was observed, which was attributed to the $P^+Q_A^- \rightarrow P \; Q_A$ charge separation. Slower phases with lifetimes of several minutes, which appeared during continuous

38

subsaturating illumination show the different stages of conformational rearrangement from dark-adapted states to light-adapted conformations. After the light was turned off, the representative kinetic traces for different illumination times also show multi-phase recovery of oxidized Bchl$_2$. Traces were analysed with three-exponential fit. The fastest kinetic component (vertical line in the kinetic trace) is attributed to the charge recombination from the dark adapted conformation, which has the lifetime of 95 ± 5 ms (Figure 3.3).
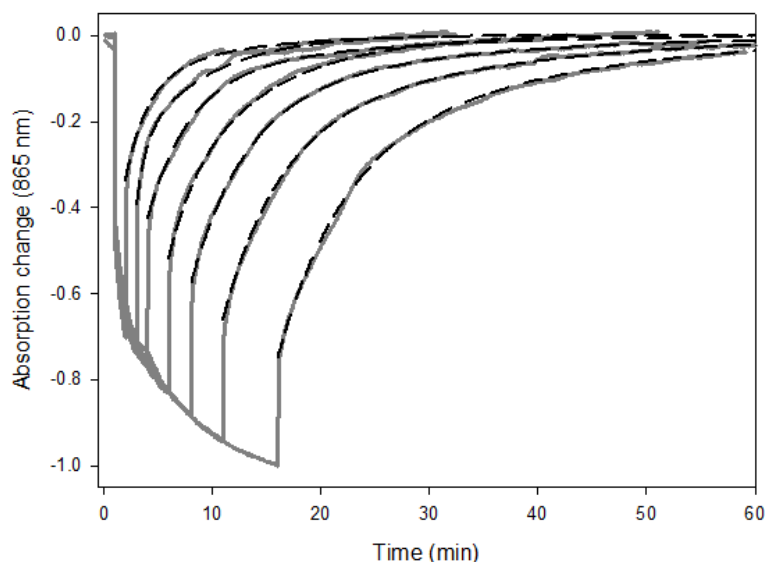
Figure 3.4 Kinetic traces of formation of long lived charge separated states upon prolonged illumination monitored at the dimer band position at 865 nm. Traces were recorded after various illumination time. The multiphasic recovery requires up to three components to describe the recovery. Traces were normalized to the trace recorded after 15 mins of illumination. The dashed curves represents the exponential fits. Rate constants are shown in Figure 3.5. Conditions: 1 μM of BRC from R-26 mutant incorporated into liposomes forms from DOPC lipids at pH 8 with 15mM Nacl and 100 μM terbutryn and 15mM Tris buffer. The tungsten lamp (80 W) was used as illumination source.

Slower components are assigned to the charge recombination from an altered conformation caused by continuous illumination. Fitting resulted lifetimes of 0.29 $\times 10^{-2} s^{-1}$ to 0.73 $\times 10^{-2} s^{-1}$ for slow and 0.8 $\times 10^{-3} s^{-1}$ to 1 $\times 10^{-3} s^{-1}$ for very slow components. After 4 minutes of illumination these rate constants became almost independent of illumination time (Figure 3.5b). At short illumination times (up to 2 minutes) the small amplitude of the slow component caused the observed rate constant to have a slightly higher value but with increasing population the accuracy to determine this parameter improved significantly. Further stabilization of the charge separated states occurs with populating the very slow kinetic component. With increasing illumination time, the amplitude of slowest component with rate constant of $\sim 10^{-3} s^{-1}$ increased from zero to $\sim 30\%$ (Figure 3.5a). After about 15 mins illumination all the amplitudes and rate constants reached their final values and did not change by further illumination indicating that they reached their equilibrium values. The independence of the rate constants of the components on the illumination time after equilibrium also indicates that these processes are first-order kinetics and do not depend on external agents. Measurements in different liposomes and in different pHs have shown the same number of components in recovery of charge separated states. The rate constant of the slow and very slow components slightly varied around $10^{-2}s^{-1}$ and $10^{-3}s^{-1}$, respectively depending on the pH and on the type of liposome (data not shown). The amplitude of the very slow component also had been strongly dependent on these factors.
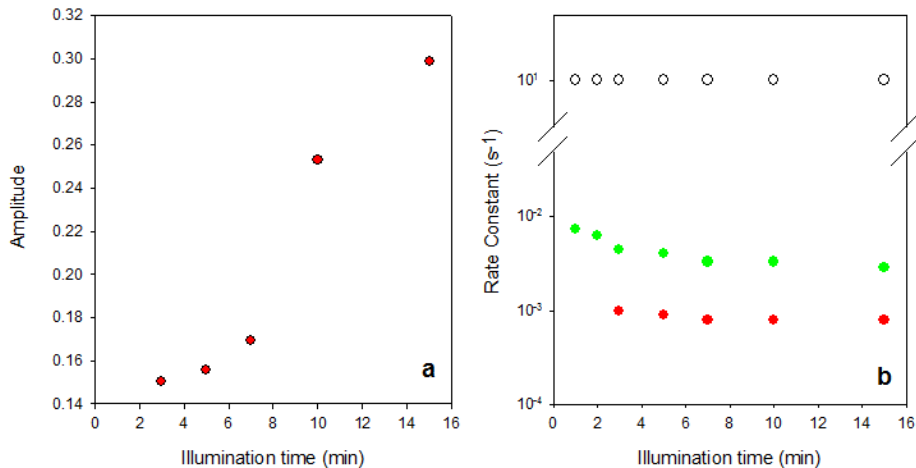
Figure 3.5 Rate constants and amplitudes of different components in the recovery kinetics of P^+ as a function of illumination time in DOPC liposomes. Traces were analysed assuming three exponentially decaying components. (a) Amplitude of slowest component as a function of illumination time and (b) rate constants of the fast (black open circles), slow (green circles), and the slowest (red circles) components . Data determined from analysis of Figure 3.4.

3.1.3 Correlation between the conformationally altered charge separated states and proton release

The stoichiometry and kinetics of proton binding/unbinding to BRC that was incorporated into liposomes formed from DOPC lipids were measured under continuous illumination. After turning off the light, the kinetics of recovery of proton release showed close rate constant as the rate constant of the slowest component (1.2×10^{-3} s^{-1} in proton release and 1.1×10^{-3}s^{-1} in charge recombination). Figure 3.6 shows the comparison between these kinetics.
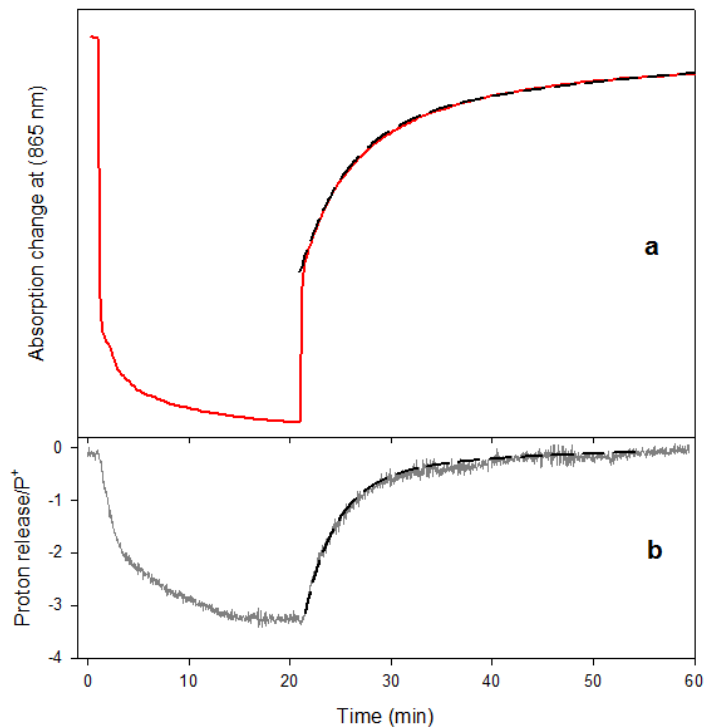
Figure 3.6 Comparison between kinetics of proton binding/unbinding and kinetics of formation and recombination of charge separated states upon prolong illumination. a. Kinetics of proton release and reuptake and b. Absorption changes monitored at dimer band position. Kinetics of deprotonation is in good agreement with slow phases of kinetics of charge recombination. The fitting parameters are explained in the text. Condition: 4 μM of BRC from R-26 mutant incorporated into liposomes forms from DOPC lipids at pH 8 with presence of 100mM NaCl and 100 μM terbutryn. The tungsten lamp (120 W) was used as an illumination source.

Kinetics of proton signals of BRCs after turning off the light with different illumination times were also recorded (Figure 3.7) and shown to be independent of illumination time (rate constant of $1.3×10^{-3}s^{-1}$ to $1.2×10^{-3}s^{-1}$ from 7 minutes to 20 minutes of illumination), which suggest that the proton release in BRC was due to the population of the longest lived charge separated state and other shorter lived conformations has little effect on proton binding/unbinding caused by illumination.
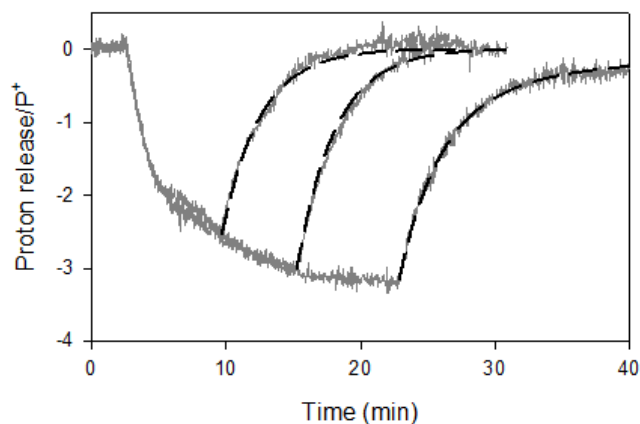
Figure 3.7 Kinetics of proton binding/unbinding after different illumination times.
Formation and recovery of these kinetics were independent of illumination time. Dashed traces represents the exponential fits with rate constants of 1.3×10^{-3} , 1.3×10^{-3} , and 1.2×10^{-3} s^{-1}. Condition as (Figure 3.6).

3.2 Effect of head group charges of lipids on the lifetime of the charge separated states

BRCs were incorporated into liposomes with different head group charges at pH 7.4 in order to study the effect of head group charge on different conformational changes in BRC. Liposomes formed from DOTAP, DOPC and DOPEG containing lipids with +1, 0, and -2 charges, respectively. The kinetics of charge recombination, spectral features and stoichiometry of light-induced proton releases were measured in all cases.

3.2.1 Relaxation of conformationally altered charge separated states upon prolonged illumination

Kinetics of charge recombination of BRCs incorporated into liposomes formed from DOTAP, DOPC and DOPEG were measured after 15 minutes of illumination at pH 7.4 and analysed with a three exponential fit.
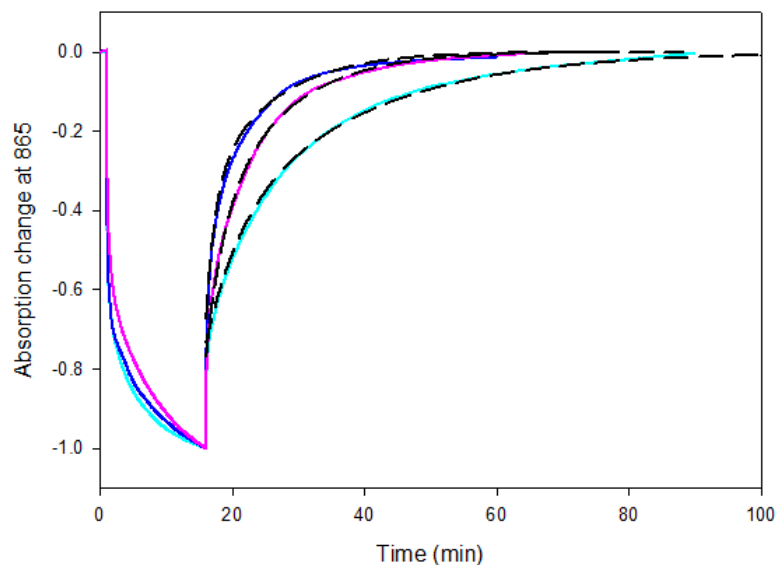
Figure 3.8 Kinetics of formation and recovery the of charge separated states of BRC incorporated into different liposomes monitored at the dimer band position at 865 nm. Traces were collected in the presence of 1 μM of BRC from R-26 mutant incorporated into liposomes forms from DOTAP (Blue), DOPC (Pink) and DOPEG (Cyan), which have +1, 0 and -2 head group charges, respectively. The illumination lasted for 15 minutes. The dashed lines represent fits using equation 2.8.1.1. The results of the fits are tabulated in Table 1. Conditions: 15mM NaCl, 100 μM terbutryn and 15mM phosphate buffer. The tungsten lamp (80 W) was used as illumination source.

Traces collected from separate measurements from two to three samples in each liposome. Representative traces have been shown as an example (Figure 3.8). Negatively charged head groups appeared to stabilize the charge separated state and positively charged head group decreased this stabilization. The rate constants and amplitudes of each component of this process are summarized in Table 1. Rate constants of the slow and very slow components were both slightly changed by the addition of different charges on lipid head groups (Figure 3.9a). The head group charge also had great influence on the amplitude of the slowest component, which is correlated with the conformational state that causes the release of protons and has a rate constant of $\sim 10^{-3} s^{-1}$. This amplitude was ~50% in case of DOPEG and was reduced to ~6% in DOTAP (Figure 3.9b).

Table 1. Rate constants and amplitudes of the components in the recovery of the charge separated states of BRC incorporated into different liposomes

Net charge	Fast	Slow		Very Slow	
	Amplitude	Amplitude	Rate constant $\times 10^2\ (s^{-1})$	Amplitude	Rate constant $\times 10^3\ (s^{-1})$
-2	0.17	0.27	0.34	0.50	0.8
0	0.19	0.36	0.65	0.45	1.6
+1	0.21	0.43	0.29	0.06	0.6

*Data determined from analysis of Figure (3.8)
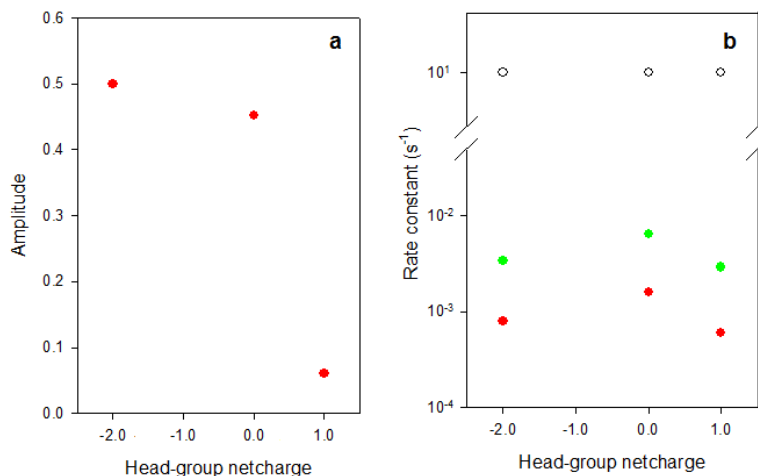
Figure 3.9 Rate constants and amplitudes of the components in the recovery of P^+ after prolonged illumination as a function of the head-group charge of the lipids. Traces were analysed with three-exponential fit. (a) Rate constants of the fast (black circles), the slow (green) and the slowest (red) components against lipids head-group charges are shown. (b) Amplitudes of the slowest (red) components (Data taken from Table 1).

Light-minus-dark difference absorption spectra were also recorded in BRC incorporated into these three types of liposomes prompt and after 4 minutes of illumination(Figure 3.10 panel A, B and C). Figure 3.10 D clearly shows the largest electrochromic absorption shifts of the absorption bands of the monomeric bacteriochlorophylls around 800 nm if the BRC is incorporated into liposomes with positively charged head groups and smallest shifts for negatively charged head groups after the 4 minutes illumination. Corresponding shifts in each individual monomer are listed in Table 2.
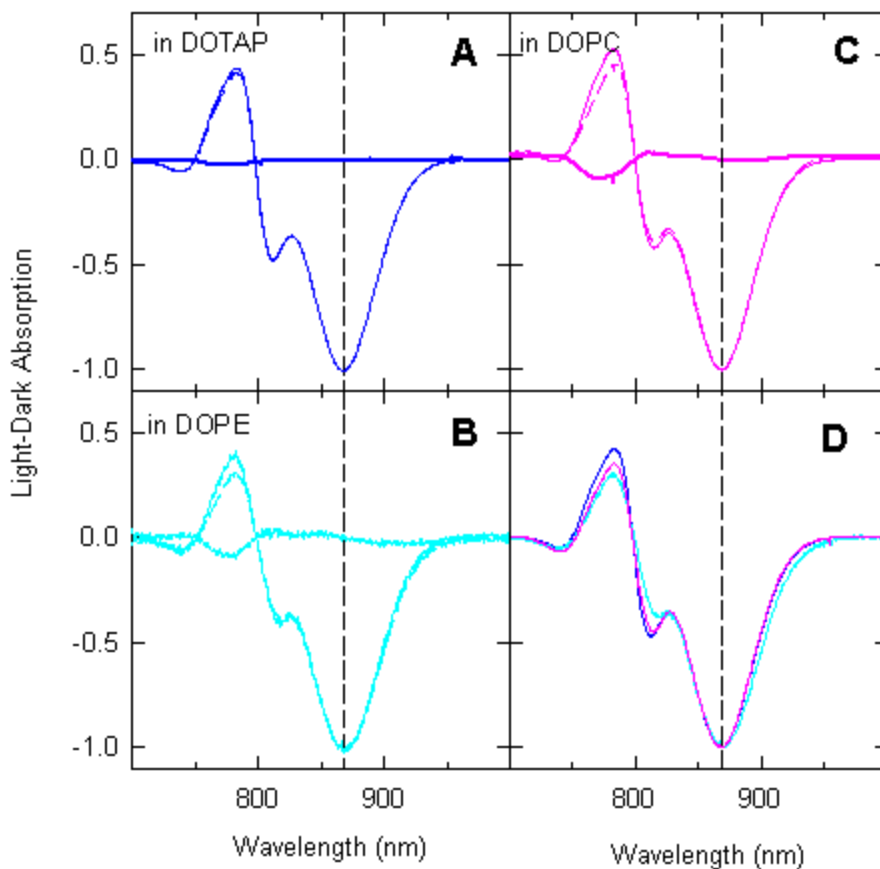
Figure 3.10 Light-minus-dark absorption difference spectra of BRC incorporated into different liposomes. Spectra were measured prompt after the illumination was turned on (solid lines) and at the end of 4 minutes of illumination (dashed lines) for (A) DOTAP, (B) DOPEG and (C) DOPEG. The vertical dashed lines at 865 nm are indicating the dimer band position. The thick solid lines are the difference between the two traces recorded at different illumination times and represent the spectral changes occurred during the prolonged illumination. The traces collected after 4 minutes of illumination are compared in panel D for all three lipids. Condition as (Figure 3.8).

The lack of relaxation (decrease) of this shift after prolonged illumination in BChl monomer absorption bands in DOTAP indicates only a degree of conformational changes in the presence of positive head group charges. The smaller electrochromic shifts in DOPC (net zero charge) and DOPEG (double negative net charge) indicate larger degree of relaxation in this order. Comparison of Figures 3.8 and 3.10 confirms that the lifetime of the charge separated state

strongly correlates with the extent of the electrochromic absorption changes of the B bands and can be used as a probe of the light-induced conformational changes. The use of lipids with negatively charged head groups resulted in a longest recovery kinetics and the greatest decrease in the electrochromic absorption changes in stabilizing the positive charge on the dimer situated just few Å from the monomers (Fig. 1.2). Data are strongly in accordance to the pervious measurement in mutants in case of the correlation between the shifts and the stability of the charge pairs [20].

Table 2 Band positions for the monomers of BRC incorporated into different liposomes in liposomes with different head group charges: Data were analysed in the dark (before the illumination), prompt after the start of the illumination, and after 4 minutes of illumination.

Net charge		$BChl_A$	$BChl_B$
+1	[a]Dark	795.2	804.16
	[b]Prompt	791.4	793.9
	[c]After 4min	791.4	794.6
0	[a]Dark	795.5	806.1
	[b]Prompt	788.8	798.6
	[c]After 4min	790.8	802.5
-2	[a]Dark	794.4	805.8
	[b]Prompt	789.5	797.6
	[c]After 4min	790.5	804.4

[a] Corresponding absorption bands before illumination

[b] Absorption band positions prompt after illumination turned on

[c] Absorption band positions after 4 minutes of illumination

3.2.2 Proton release from BRCs incorporated into liposome with different head-group charges

Light induced proton binding/unbinding of BRCs reconstituted into DOPC, DOPEG and DOTAP were measured after 20 minutes prolonged illumination at pH 7.4. Representative traces have been shown in Figure 3.11. Stoichiometry of proton release was different from 0.3 protons/P^+ for DOTAP to 4.3 and 7.0 protons for DOPC and DOPEG, respectively.
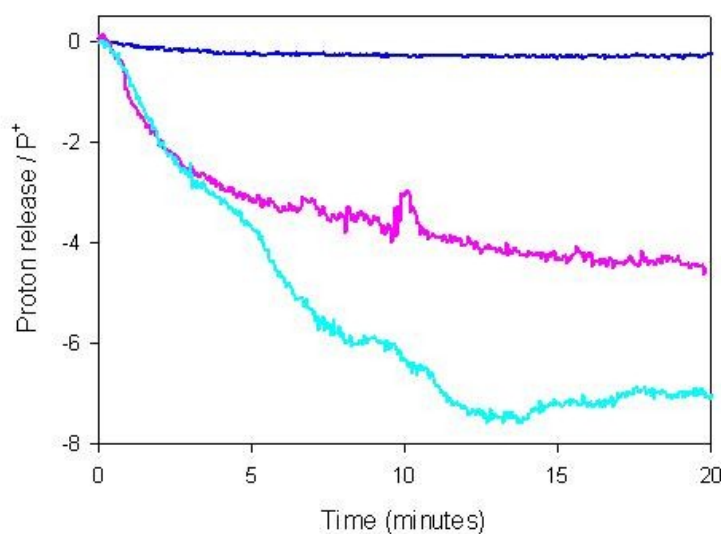
Figure 3.11 Effect of the lipid head-group charge on stoichiometry of proton release in BRC. Proton release due to 20 minutes prolonged illumination from BRCs incorporated into DOTAP (Blue), DOPC (Pink) and DOPEG (Cyan) at pH 7.4. For DOTAP, DOPC and DOPEG the following values were obtained 0.3 ,4.3, and 7.0, respectively. Conditions: 4 μM BRC in DOPEG, DOPC and DOTAP liposomes with 100mM NaCl and 100 μM terbutryne.

The extent of the proton release also correlates with the lifetime of the longest lived component of the charge separated state. Larger amplitude of the kinetic component with the ~10^{-3} s^{-1} rate constant resulted in larger proton release.

3.3 pH-dependency of charge separated states in BRC incorporated into liposomes.

Kinetics of the formation and recovery of the charge separated states were measured in BRCs incorporated into DOPC liposomes by monitoring the absorption changes at dimer band position at several pH values from 6 to 10 in two sperated samples for each pH. Figure 3.12 shows the difference in charge recombination in two different pHs (pH 10 and 7.4) as an example. Analysis of recombination of these conformationally altered charge separated states revealed components with different lifetimes and amplitudes, which are strongly dependent on pH of environment of BRC.

This figure clearly shows that after 15 minutes of illumination the oxidized bacteriochlorophyll dimer needs about 45 minutes to recover at pH 7.4 while at pH 10 this required time will reduce to 15 minutes. The parameters of the analyses of these kinetic traces are summarized in Table 3.
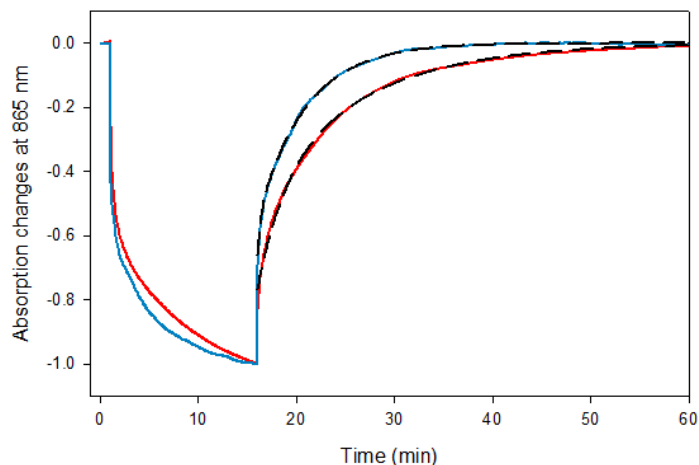
Figure 3.12 Representative kinetic traces of the formation and recovery of charge separated states of BRC incorporated into DOPC at pH 7.4 (red curve) and 10.0 (blue curve)**.** Dashed lines represent the fits using equation 2.8.1.1. Condition: 1 μM of BRC from R-26 mutant in 15mM NaCl , 100 μM terbutryn and 15mM phosphate buffer for pH 7.4 , 15mM CAPS for pH 10. The tungsten lamp (80 W) was used as illumination source. The results of the analyses for the entire pH range is shown in Table 3.

Table 3. Rate constant and amplitude of each component in the recovery of charge separated states of BRCs incorporated into DOPC in different pH values.

pH	Fast	Slow		Very Slow	
	Amplitude	Amplitude	Rate constant $\times 10^2 \, (s^{-1})$	Amplitude	Rate constant $\times 10^3 \, (s^{-1})$
6.2	0.32	0.39	0.43	0.29	0.5
7.4	0.19	0.36	0.65	0.45	1.6
8	0.25	0.45	0.29	0.30	0.8
9	0.24	0.58	0.24	0.18	0.6
10	0.33	0.62	0.35	0.05	1.4

In Figure 3.13 we compare the amplitude of slowest component as a function of the pH. This amplitude increased from ~5% at pH 10 to about ~45% at pH 7.4 and again decreased towards more acidic ranges. From Figure 3.13 we can predict that the population of the slowest component should have a peak somewhere between pH 7.4 to 6.2.
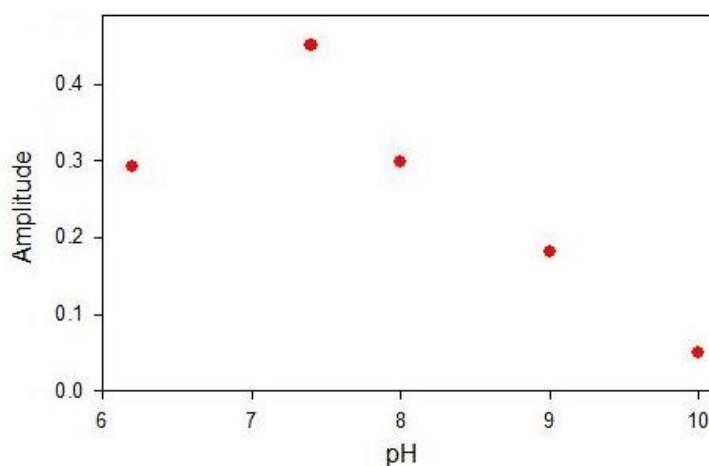
Figure 3.13 Amplitude of slowest component in the recovery kinetics of P^+ after prolonged illumination as a function of pH. Data taken from Table 3.

Stoichiometry of proton release caused by prolonged illumination was measured in BRCs reconstituted into DOPC, DOPEG and DOTAP in different pHs from 6 to 9 (Figure 3.14) and were compared with results that were measured earlier in Triton X-100 detergent (non-ionic with zero net charge) micelles [15].

Data has been fitted with the difference of two Henderson-Hasselbalch-type curves with fixed number of protonation groups of 16. Protonable residues assumed to have the same *pKa-s* in this analysis. Stoichiometry of proton release

was very similar for DOPEG and DOPC (~7.5 and ~7.2 protons) and estimated to be almost the same for DOTAP.
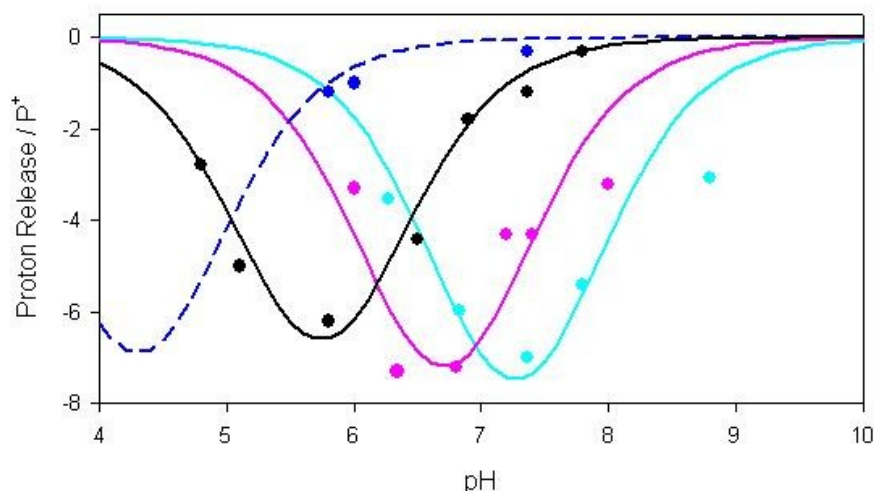
Figure 3.14 pH-dependency of the light induced proton release in different liposomes and detergent micelles. Stoichiometry of proton release in DOPEG (cyan circles), DOPC (pink circles) and in DOTAP (Blue circles) compared to those measured in Triton X -100 at various pH values Solid lines represent the fits using eq.1.8.2.2. Parameters of the fits are explained in the text. Condition: 4 μM BRC incorporated into liposomes with 100 mM NaCl and 100 μM terbutryn.

Data could not be gathered at pH values below 5.8 for DOTAP due to instability of the protein in this liposome. The peak positions for the proton release were completely different and increased to more alkaline pHs with increasing negatively charges on the lipid head-groups. Also the peak position of DOPC, which is neutral in these pHs is about 1 pH unit higher than in Triton X-100, which is a neutral detergent. From the analysis, *pKa* values of residues have been modeled to be shifted from 6.15, 7.13, 7.71 to 5.33, 6.29, and 6.83 for Triton, DOPC and DOPEG respectively.

4. Discussion

In my thesis work, proton release, light induced spectral changes of the primary charge pair and kinetics of charge recombination were measured in BRC exposed to continuous illumination. Large differences in the recovery of charge separated states and in the light-induced proton release were observed, which are caused by the systematic changes introduced in the environment of BRC. The systematic changes were to alter the head group charges of the liposomes that the BRC was incorporated in and altering the pH, which influences the total number of surface charges of the RC protein as the protonational state of the amino acid side chains with protonatable side chains changes. These alterations in the function of BRC were also correlated to the light-induced spectral changes, which can be understood on the basis of structural changes in BRC upon illumination. The discussion will focus on the origin of proton release caused by the conformational changes in BRC at molecular level and the effect of the environment of BRC on these conformations. A strong correlation was found between electrochromic absorption changes in light-minus-dark difference optical spectra and the recovery kinetics of the charge separated states and the extent of the proton release, when the BRC was placed to different environments.

4.1 Molecular assignment of the light-induced conformational changes

To study the function of BRC in different light-induced conformationally altered states, we varied the illumination time from single flash excitation to several minutes of illumination.

In the presence of an inhibitor, the flash induced $P^+Q_A^- \rightarrow PQ_A$ charge recombination is expected to be a single exponential decay [36] because the quantum yields of conformational changes were found to be low and not be detectable after flash excitation. The rate constant for this process is about $10s^{-1}$ in case of wild type BRC in detergent [37]. In our project, we have measured this rate constant slightly larger than those found in detergent micelles when the BRC was incorporated into liposomes (Figure 3.3). The increase of the rate constant in liposomes was also reported earlier in liposomes with different lipids (phosphatydylethanolamines) [38]. Upon prolonged illumination the conformationally altered states can be built up (Figure 3.4 and 3.5) as they have longer lifetimes than the charge recombination from the dark-adapted conformations. The longer lifetimes determined using prolonged illumination were attributed to the recombination of the charge pairs in BRCs that adapt these different conformations induced by the light.

The lifetime and number of kinetic components were also varied depending on conditions, such as pH and hydrophobic environment of the BRC [15, 19], which indicates different level of stabilization of the charge separated state in different conformations. In this work, up to 4 components with several orders of magnitude differences in their lifetimes were distinguished that are characteristic to the dark-

adapted and three different light-adapted conformations (Figure 3.5 and 3.9). Up to very recently the individual conformational changes with different lifetimes have not been identified completely at molecular level, although some of the studies proposed conformational changes near quinones [14-18]. This assumption was mainly supported by X-ray crystallographic studies but these studies used very short illumination (less than a second) to generate light-induced states. It is obvious from this work as well as earlier studies that accumulation of long-lived states requires much longer illumination. [15, 20, 39]. The recent reports from our group provided evidence for structural changes around the dimer. These changes were identified as displacements of the internal water molecules and changes in local dielectric constant due to the light-induced alterations of the hydrogen bonding pattern between the M210 Tyr residue and the 2-acetyl group of the M-half of the dimer, which resulted in a decrease of the redox midpoint potential of the dimer [20]. The conformational changes were also linked to an opening of a slow proton pathway, which is triggered by the deprotonation of the Tyr M210 residue [38]. The observed pH dependent proton release was explained as a response to the shifts of the *pKa* values of the protonatable residues around the dimer caused by the light-induced increase of the local dielectric constant in the vicinity of the proton releasing amino-acids [15, 39].

4.1.1 Changes of P/P^+ midpoint potential due to the structural changes

The $P^+Q_A^- \rightarrow PQ_A$ charge recombination process, which is non-adiabatic electron transfer, takes place over a large range of 25 Å. This process is a quantum jump between the parabolic potential energy surfaces of the reactants and products deducted from the Marcus-theory of electron transfer (Figure 1.3) The free energy difference between the initial $P^+Q_A^-$ state and the final $P\ Q_A$ state ($-\Delta G_0$) was approximately 500 meV in wild-type BRCs and the reorganization energy was modeled and reported as 930 meV at room temperature [40].

The lifetime of the $P^+Q_A^-$ charge-separated state could be changed by altering the free energy difference between $P^+Q_A^-$ and $P\ Q_A$ states, for example in some mutant studies, the rate constant of the $P^+Q_A^- \rightarrow PQ_A$ charge recombination after flash excitation as expected from Marcus-theory followed the dependence on P/P^+ midpoint potential, which was altered by introducing or removing hydrogen bonds to the dimer [37]. This potential in the presence of a weak illumination has been decreased by 75 mV in a large fraction of BRCs in detergent micelles [20]. This decrease was found to be 35 mV and 110 mV in case of BRCs incorporated into DOTAP and DOPC liposomes, respectively (measured by our Colleague Sasmit Deshmukh). Such a large shift in the potential of dimer should originate from either within or from the immediate vicinity of BChl molecules caused by the light induced structural changes. For example the P/P^+ potential was shown to be regulated by the protonational states of introduced Asp

and Glu residues within 6 Å from P [42]. Deprotonation of these residues in high pH caused the midpoint potential to drop by about 60 mV. In wild type BRC, however, there are very few amino acids with protonatable side chains in immediate vicinity of P. The most likely candidate for the strong interaction is Tyr M210 (Figure 3.1), which is in van der Waals contact with one half of the dimer and the local dielectric constant was reported to be less than 4.7 in that region, which is a favourable condition for pKa shift upon oxidation of dimer [7, 39].
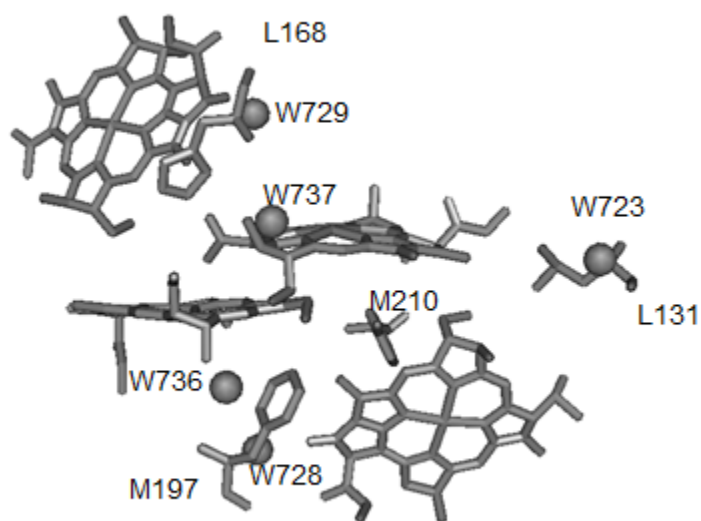
Figure 4.1: Structural view of BChl$_2$ and with nearby amino acid residues and internal water molecules. Five water molecules (W728, W729, W737, W723 and W736) were shown in immediate vicinity of BChl$_2$ with their nearby residues. Tyr M210 is also shown. Coordinated were taken from reference X using PDB entry code: 4RCR [43].

4.1.2 Correlation between the increase of the local dielectric constant and the light-induced proton release

Prolonged continuous illumination generated states in different fractions of the BRCs whose recovery was no longer following the classical Marcus-theory for the rate constants, which indicates that the rate constants must be limited by other factors, such as the rate of protonation or conformational changes. It has been reported earlier that light induced structural changes alter the local dielectric constant near $BChl_2$ [20]. Mutant studies presented evidence that these dielectric changes are mainly due to the changes in spin density distribution between two half of the $BChl_2$ [39] and displacement of internal water molecules, as the rotation of the 2-acetyl group of the dimer was identified earlier to alter the shring of the electron hole between the two halves of P [42]. One of the X-ray crystal structures of the BRC identified five water molecules (W728, W729, W737, W723 and W736) in the near vicinity of the four BChl that are in interaction with some of the residues like L131, M197 and L168 in key position in terms of their potential to influence the electrochromic absorption changes (Figure 4.1) These water molecules are aligned with the transition dipoles of $BChl_2$ and one of the BChl monomers. Displacement of these water molecules will cause changes in local dielectric constant and different pattern in their H-bonding. Because the interaction energy causing the electrochromic absorption changes are inversely proportional to the dielectric constant, any significant change in local dielectric constant is causing a change in the electrochromic absorption shifts of the BChl

monomers (Figure 3.2). Analysis shows the electrochromic shift in $BChl_B$ was about twice larger than the shift in $BChl_A$ (Figure 3.1 and Table 3) prompt after illumination when very small fraction of BRCs experienced conformational changes near the dimer. This difference is mainly due to the larger dielectric constant near $BChl_A$ than $BChl_B$ [7]. Continuous illumination causes decrease in the electrochromic absorption change in BChl monomer bands. The decrease of the electrochromic absorption changes upon prolonged illumination was also accompanied by a formation of the same but longer lived charge separated state (Figure 3.2 and 3.5). Extent of this dielectric relaxation was also correlated with the increase of the amplitude of long lived states. (Figure 3.8 and 3.10). For example, after 4 minutes of illumination the electrochromic shift in $BChl_B$ band in BRC incorporated into DOPEG was reduced by 6.8 nm, which is an indication of the increase of the local dielectric constant by the light induced structural changes in that region. This reduction was 3.9 nm in DOPC and only 0.7 nm in DOTAP, where the charge separated state has shorter lifetimes. The behaviour of the BRC in the positively charged DOTAP liposomes (nearly negligible decrease of the electrochromic absorption changes (Fig. 3.10), shorter lifetime of the charge separated state (Fig. 3.8), and the lack of significant proton release (Fig. 3.11) resembled the behaviour of a mutant, where the hydrophobic and neutral Leu residue at the L131 position was replaced by the hydrophilic, positively charged His [20, 39]. In this mutant the introduction of the positively charged His blocked the conformational changes. We conclude that the positively charged

60

DOTAP also should prevent the formation of the long lived conformations even in the native reaction centers at neutral pH at 7.4.

The other consequence of dielectric relaxation of BRC upon prolonged illumination is altering the *pKa* values of protonatabe amino acids around the $BChl_2$. The new conformations of the protein weaken the electrostatic interaction of P^+ with the protonatable residues of the BRC, which in turn will have their *pKa* values shifted causing light-induced proton release from periplasmic side of BRC. Experimental evidence shows that the rate constant of charge recombination in the longest lived state is limited by the rate of these protonation [39].

The recovery of light-induced proton release had monophasic behavior with rate constant of about 1.2×10^{-3} s^{-1}, which was independent of the illumination time (Figure 3.6 and 3.7). The stoichiometry of proton release was also correlated with the amplitude of the longest-lived state with the same rate constant (Figure 3.5a). The component with rate constant of $\sim 10^{-3}$ s^{-1} is the result of the additional stabilization of the charge separated state with proton release in the light-adapted conformation. Since the proton release is not coupled with additional decrease of neither the P/P^+ potential nor the electrochromic absorption changes of the monomer bands [20, 39] most of the proton releasing residues must not be in the immediate vicinity of $BChl_2$ or the BChl monomers. There are a total of 14 Glu, Asp, and His residues that are at least 10 Å away from the $BChl_2$ on the periplasmic side of the BRC and their *pKa* changes may account for the proton release. The stoichiometry of proton release is not only limited by the number of available protonatable groups but also by the energetic coupling of the residues

and the interaction with groups that are already deprotonated. The loss of positive charge on the protonated residue upon deprotonation, however, can be screened by external ions; so larger ionic strength of the solution should cause larger proton release, which is supported by salt titration experiments of the proton release [15]. There is another limitation for the amount of the light-induced proton release in BRC. The light-induced shifts in *pKa-s* of the residues in the periplasmic side is less than one pH unit (Figure 3.14), but not all the *pKa–s* of residues are in the investigated pH range to cause releasing protons. To build long-lived charge separated states we systematically altered the *pKa* of these amino-acids to bring them to the investigated pH range with some changes in the environment of the BRC like incorporation into more hydrophobic environment or introducing external charges near the protonatable residues. These changes were caused the stoichiometry of proton release to change from 0.3 to about 7 per P^+ (Figure 3.11).

4.2 Effect of the environment of BRC on light-induced proton release

The environment of BRC can alter the *pKa-s* of the protonatable amino acids by two major effects; Altering the local dielectric constant and introducing charges nearby. Earlier studies indicated that the dielectric constant inside the detergent micelles is less than that of water and the *pKa* of acidic indicators incorporated into these micelles were shifted towards higher values [26]. Also, the presence of positive and negative charges on head groups of the detergents decrease and

increase the *pKa* values, respectively, of the acid-base indicators embedded into these detergent micelles. For example the *pKa* of one of the indicators, which was 7.75 in aqueous bulk solution increased to 8.85 when it was incorporated into Triton X-100, which is a neutral detergent. This shift was due to the lower dielectric constant inside the Triton X-100 micelle than water. On the other hand the *pKa* of the same indicator increased to 11.15 in SDS (sodium-dodecyl-sulfate), which is a negatively charged detergent. Incorporating this indicator into CTAB, a positively charged detergent, caused the *pKa* to decrease to 6.35, which is even less than what it was in aqueous solution. In this project, a similar effect was detected in the *pKa-s* of protonatable amino acids on the periplasmic side of BRC when the BRC was incorporated into liposomes with different head group charges. The consequence of these shifts can be detected by the correlation between the stoichiometry of the light induced proton release from BRC and the amplitude of the longest-lived charge separated state. For example, at pH 7.4, the BRC incorporated into liposomes with different head group charges show different lifetimes in recovery of charge separated states after prolonged illumination (Figure 3.8). These differences are mainly due to the differences in the population of the longest-lived state with rate constant of $\sim 10^{-3} \text{s}^{-1}$ (Figure 3.9a), which is correlated with extent of proton release from BRC. For example the population of this state was about 50 % in DOPEG (negatively charged lipid) and 7.0 H^+/RC was measured at pH 7.4. The same component was present only in 6 % of the BRCs in DOTAP and only 0.3 H^+/RC was detected at the same pH. These differences in the population of the component with rate constant of 10^{-3} s^{-1}

is mainly due to the number of available protonatable residues, that experienced *pKa* shifts and also the extent of the shift itself. The large difference in stoichiometry of proton release, thus is most likely due to the effect of the head group charges on the *pKa* of acidic amino acids near P^+.

The changes in the population of the state with rate constant of $\sim 10^{-3}\ s^{-1}$ can also be detected when pH-dependency of the recovery of the charge separated state was measured in liposomes from DOPC, which has a zwitterionic head group (Figure 3.13). In this particular liposome the population of this state decreased from 45 to 5 % as the pH was raised from 7.4 to 10.0 and also deceased as the pH was lowered from pH 7.4 to pH 6. This will suggest that *pKa* of protonatable residues are mainly around pH 7.4. This effect will result in a faster recovery of charge separated state at pH 10 than in the other pH values (Figure 3.12). pH-dependency measurement of recovery of the charge separated state and proton release could open the way to measure the *pKa-s* of these residues in each particular liposome..

As it was discussed earlier, negative charges near acidic amino acids will increase the *pKa* of these residues toward higher values and presence of positive charges nearby will shifts these *pKa-s* to the more acidic pH. The presence of positive and negative charges on head groups of DOPEG and DOTAP lipids may cause the same effect on the protonatable residues in the periplasmic side of BRC. The pH dependency of the proton release measurement is supporting this assumption by recording different pH for the maximum of the light-induced proton release in

liposomes with different head group charges (Figure 3.14). The *pKa* of acidic amino acids, which are usually Asp and Glu on the periplasmic side, was measured to be 7.71, 7.13 and estimated to be 4.5 in DOPEG, DOPC and DOTAP respectively (Figure 3.14). These *pKa-s* were assumed to be the same for all of these residues in the analysis for simplicity following the example introduced in reference [26]. Presence of positively and negatively charged head groups of lipids shifted the *pKa* of these residues in a wide range of 3.2 pH units, however, these charges did not influence the interaction between P^+ and these residues significantly. The light induced shift in these *pKa* was almost the same for all these liposomes (about 0.85 pH units). The best fitting to the difference of two Henderson-Hasselbalch curves (Figure 1.10 and 3.14) achieved by assuming 16 active protonatable groups in the periplasmic side, which is slightly more than the number of available protonatable residues in this region. This difference may be caused from the difference between proton activity coefficients near the surface of BRC and the aqueous solution. The proton activity coefficient was reported to be sensitive to the dielectric environment. For example the activity coefficient is about 0.33 in 0.03% Triton X-100 dispersion and ~1.00 in diluted aqueous solutions [15]. The difference in proton activity between the surface of BRC and aqueous solution will cause the released proton, from the surface to the bulk, to be counted more by the pH electrode.

The other factor, which may influence the *pKa* of the residues, is the effect of the liposome membrane on the local dielectric constant, which can alter the self energy of these amino acids. Crystal structures are available on detergent isolated

BRC at atomic resolution. In one structure [5], the detergent belt was found about 5Å thinner than the length of transmembrane helices in BRC (Figure 1.4). On the other hand the thickness of lipid bilayer in all type of liposomes in this study is slightly thicker than the length of α-helices [47]. Earlier studies showed that the local dielectric constant inside Triton X-100 micelles is about 30 [26]. This dielectric constant is lower in liposomes (~10 to 30) even at the surface of the vesicle [45]. The thicker lipid bilayer with lower dielectric constant in liposomes compared to the detergent belt will cause lower local dielectric constant inside the BRC, which can shift the *pKa* values of protonatable groups to the higher pHs. This can be seen in Fig. 3.14 where the maximum of the light-induced proton release in DOPC and Triton X-100, which have both neutral head groups are different. The maximum proton release was observed at about pH 5.8 in Triton X-100 but it sifted to pH 6.8 in DOPC indicating that the local dielectric environment of the proton releasing residues is different.

4.3 Assigning the kinetic components to conformational changes

I adopt a model (Scheme 1) that explains the results of this work and other works by our research group, developed by my fellow student colleague, Sasmit Deshmukh, which uses minimum of assumptions [20, 39].
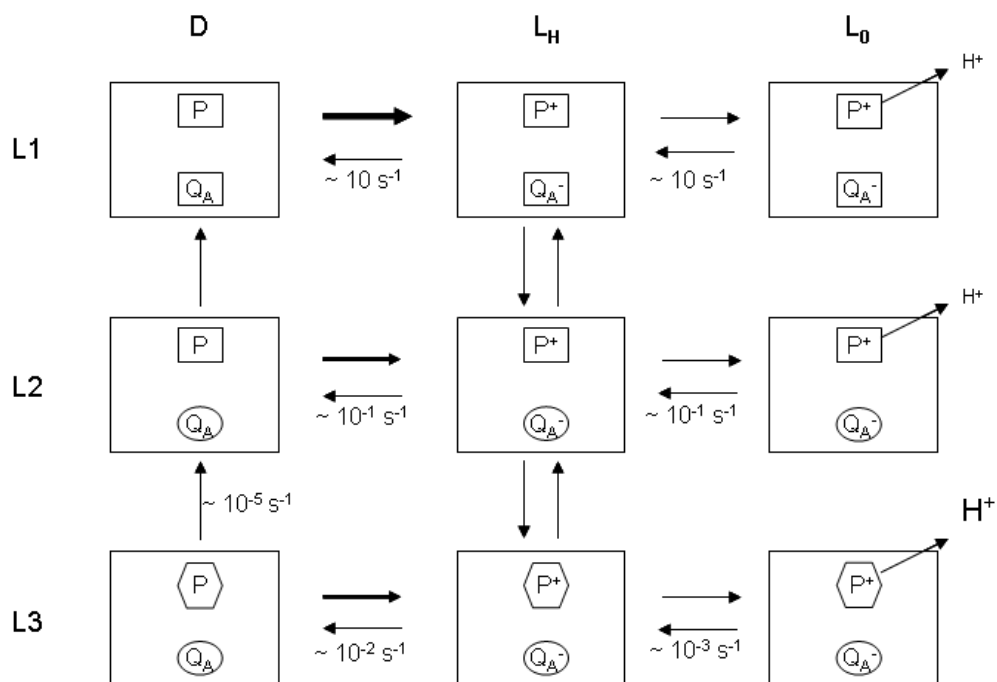
Scheme 1 Minimal model of the light-induced and redox reactions, conformational, and protonational changes in BRCs. Explanation is found in the text**.** Figure was modified from [38].

In the scheme the horizontal displacements are redox reactions (D →L_H) and deprotonational steps (L_H →L_0),

and the vertical displacements are structural changes from a dark-adapted conformation (L1), to an intermediate and final light-adapted conformation (L2 and L3). In dark adapted samples (L1) the charge separation forms the $P^+Q_A^-$ state and the recombination takes place in ~ 100 ms (Figure 3.3). Due to the very low quantum yield of the conformational changes, multiple turnovers are needed to build up the other conformational levels indicated by L2 and L3. The multiple turnovers achieved by continuous illumination in this study. The populations of

the different conformational levels are dependent upon the illumination time, pH and the environment of BRC (Figure 3.5 and 3.9). At very short illumination times (~1s) the component with a rate constant of ~$10^{-1}s^{-1}$ is the first to appear in the recovery kinetics among the slower components but amplitude of this component is not detectable even after one minute of illumination in our samples except in few of those, which the amplitude of the conformations in L3 were less than 50 present. Earlier studies proposed that the component with a rate constant of ~$10^{-1}s^{-1}$ is most likely due to the recovery of P^+ caused by the light-induced conformational changes taking place in the vicinity of the quinones, at the cytoplasmic side of the RC [15, 20]. This assignment is in agreement with the X-ray crystallographic studies where after a short illumination (< 1 s) structural changes were reported near the quinones [45, 46]. Population of the slow component with rate constants of ~10^{-2} s^{-1} at level L3 (Figure 3.9 and 3.5) was accompanied by decreased electrochromic absorption changes of the BChl monomer band upon illumination (Figure 3.2 and 3.10) that was assigned to the increase of the local dielectric constant [20]. We assigned the L3 level as the conformational state formed due to structural changes occurring at the periplasmic side, near P. As the amplitude of the very slow component with a rate constant of ~10^{-3} s^{-1} (Figure 3.9 and 3.5) was correlated with the extent of the proton release, it has been concluded that this component should also arise from conformational changes at the periplasmic side but from a different protonational state [38]. The matching kinetics of the recovery of the proton release and the recovery of the charge separated state (Figure 3.6) indicates that the re-protonation step is rate

limiting at the L3 level. After flash excitation, at the L1 level, the kinetics of the re-uptake of the substoichiometric proton release was also found the same as the charge recombination [23]. While the proton release in the dark-adapted conformation (at L1 level) after a single flash excitation is also caused by the shift of the *pKa-s* of the nearby residues it can only be substoichiometric since it is due the interaction of the single positive charge on P with the protonatable side chains [23, 24]. This can only provide very moderate stabilization for P^+ due to proton release. At level L3, however, the increased value of the dielectric constant upon structural changes can shift the *pKa-s* of many residues significantly resulting in a large proton release and longer lifetime of the charge separated state [39].

According to the proposed Scheme 1 there are two different conformations of P: the dark adapted conformation at levels L1 and L2 (indicated by squares) and the light-adapted conformation, at level L3 (shown as hexagons). The relaxation time from L3 to the L2 (or L1) conformational level in the ground state was reported to be approximately 6 hours (rate constant of $\sim 10^{-5}$ s-1) after prolonged illumination and about one hour after 1 minute illumination in RCs dispersed in LDAO micelles [20, 39].

5. Conclusion

In summary we have shown that the rate of the recovery of the oxidized dimer in the $P^+Q_A^-$ state depends systematically on the protein environment of P^+. The extension of the lifetime of the charge separated state by up to four orders of magnitude via light-induced structural and protonational changes provides new opportunities to utilize the BRC in energy storage as a biocapacitor. The charges separated over ~20 Å distance in a low dielectric constant medium can be prevented from recombination by systematic alteration of the environment of the charges and the light can be used as a switch. We have systematically altered the environment of BRC by incorporating it into different liposomes to populate the state with the longest lifetime of ~10^{-3} s^{-1}. The relative population of this state was correlated with the extent of light-induced proton release from BRC. The charge separated state in BRC incorporated into liposomes with negatively charged head groups showed the longest life time in the recombination process in comparison with neutral and positively charged liposomes. The extent of the light-induced proton release was found to be strongly dependent on the interaction of head groups of the membrane forming lipids with the protonatable residues at the periplasmic side of BRC. It was also sensitive to the hydrophobic interactions between the fatty acid chains of the lipids and the BRC protein. I have determined that most likely all protonatable residues at the periplasmic site participate in the light-induced proton release regardless of the charge of the head group. The pH at which the maximum proton release is measured, however, is primarily set by the

head-group charges of the lipids of the surrounding liposomes. At neutral pH the extent of the conformational changes were found significantly dependent on the head group charge as these charges shift the *pKa* values of the periplasmic residues towards different directions and by differnt extent along the pH scale.

6. Future Work

This project can further be extended in order to increase the lifetime of the charge separated state by

    i.   Further decreasing the dielectric constant of the environment of BRC by incorporating it into polymers, which can further increase the population of longest lived charge separated state.

    ii.   Altering the ionic strength of the sample. On one hand the charge on the amino acid residues can be screened by external ions and increasing ionic strength should result in larger proton release, since it minimizes the electrostatic interactions between the charged residues. On the other hand high ionic strength can also screen the charges on the head groups of the lipids. Finding the optimum ionic strength which maximimizes the population of longest lived state is a key to map the effect of the local electrostatics in BRC

    iii.   Using lipids with different hydrophobic thickness. Influence of the hydrophobic mismatch caused by the differences in thicknesses between the lipid and the BRC can answer why the properties of the BRCs are different in detergent isolated forms and in the natural membrane environment.

References

1.   Bacon, Ke, *Advances in photosynthesis*, **chapter 11**, *Vol 10*, 199-212.

2.   Allen, J.P. *et al*. *Proc. Natl. Acad. Sci. U. S. A*, **1987**, *84*, 6162-6166.

3.   Allen, J.P. *et al*. *Proc. Natl. Acad. Sci. U. S. A,* **1987**, *84,* 5730-5734.

4.   Komiya, H. *et al*. *Proc. Natl. Acad. Sci. U. S. A A*, **1988**, *85,* 7993-7997

5.   Roth, B. *et al*. *Biochemistry*, **1991**, *30,* 9403-9413

6.   Milton J. Rosen, *Surfactants and Interfacial Phenomena, WHILEY-ITERSIENCE, 3rd edition,* **2004**, Chapter 3, 105-136.

7.   Steffen, M *et al*. *Science,* **1994***, 264*, 810-816.

8.   Camara-Artigas *et al*. *Proc. Natl. Acad. Sci. U. S. A.*, **2002**, *99,* 11055-11060.

9.   McPherson, P.H. *et al*. *Biochim. Biophys. Acta*, **1990**, *1016*, 289-292.

10.   Paddock, M. L. *et al*. *Proc. Natl. Acad. Sci. U. S. A*, **1989**, *86*, 6602-6606.

11.   Axelrod, H. L. *et al*. *Photosynth. Res.*, **2005**, *85,* 101-114.

12.   Miller, J. R. *et al, Chem Soc,* **1984***, 106 ,* 3047

13.   Kleinfeld, D. *et al, Biochemistry*, **1984**, *23 ,* 5780-5786

14.   Goushcha, A. *et al*. *J. Phys. Chem B*, **1997**, *101*, 259–265.

15.   Kálmán, L. *et al*. *Biochemistry,* **1997,** *36,* 15269-15276

16.   van Mourik, F. *et al*. *Biochim. Biophys. Acta*, **2001**, *1504,* 311-318.

17.   Xu, Q. *et al*. *Biochemistry*, **2001**, *40*, 3232–3241.

18.   Andreasson, U. *et al*. *Photosynth. Res*, **2003**, *75*, 223–233.

19.   Olenchuk, M. *et al*. *Mol. Cryst. Liq. Cryst*, **2008**, *497*, 121–128.

20.   Deshmukh, S. S. *et al. Biochemistry* **2011***, 50,* 340-348

21.   Cramer, W. *et al.   Energy Transductionin Biological Membranes*, Springer-Verlag **1990**, New York.

22.   Maróti, P. *et al. Progress in Photosynthesis Research*, **1987***, 2*, 401-404.

23.   Maróti, P. *et al. Biochim. Biophys. Acta,* **1988**a, *934*, 314-328.

24.   McPherson, P. *et al. Biochim. Biophys. Acta,* **1988**, *934*, 348-368.

25.   Kensal, E. *et al. Principles of Physical Biochemistry, PEARSON,* **2006**, Chapter 2, 16-19.

26.   Marta, S. *et al. J. Phys. Chem.* **1997**, *81*, 1755-1761

27.   McMahon, B. *et al. Biophys. J.* **1997**, *72*, A418.

28.   Beroza, P. *et al. The Photosynthetic Bacterial Reaction Center II: Structure, Spectroscopy and Dynamics* (Breton, J., and Vermeglio, A., Eds.), Plenum Press, New York and London, **1992**, 363-374

29.   Beroza, P. *et al. Biophys. J,* **1995**, *68*, 2233-2250.

30.   Gunner, M. *et al. Proc. Natl. Acad. Sci. U. S. A,* **1991,** *88*, 9151-9155.

31.   Gunner, M. *et al. The Photosynthetic Bacterial Reaction Center II: Structure, Spectroscopy and Dynamics* (Breton, J., and Vermeglio, A., Eds.), Plenum Press, New York and London, **1992**, 403-410

32.   Lancaster, C. *et al. Biophys. J.* **1996**, *70*, 2469-2492.

33.   Clayton, R. K. *et al. Photosynth Res*, **2000**, *73,* 63-71

34.   Feher, G. *et al. The photosynthetic bacteria. Plenum Press, New York*, **1978**, 349–386

35.   Trotta, M. *et al. Int. J. Pharm,* **2002**, *241*, 319–327

36.   Kleinfeld, D. *et al*. *Biochim. Biophys. Acta,* **1984**, *766*, 126–140.

37.   Lin, X. *et al*. *Proc. Natl. Acad. Sci. U. S. A*, **1994**, *91*, 10265–10269.

38.   Agostino, A. *et al. Photosynth Res,* **2005**, *83*, 53-61

39.   Deshmukh S. S *et al. Biochemistry* **2011***, in press*

40.   Ortega, J. M. *et al. Biochemistry,* **1996** , *35,* 3354-3361

41.   Williams, J. *et al*. *Biochemistry*, **1992**, *31*, 11029–11037.

42.   Rautter, J. *et al*. *Biochemistry,* **1995**, *34*, 8130-8143.

43.   Ermler, U. *et al*. *Structure*, **1994**, 2, 925–936.

44.   Francis, C. *et al. Biophys. J,* **1986**, *49*, 459-468

45.   Stowell, M. *et al. Science,* **1997**, *276,* 812-816.

46.   Katona, G. *et al*. *Nature Struct. Mol. Biol,* **2005**, *12*, 630-631.

47.   McIntosh, T. *et al. Biochim. Biophys. Acta*, **1980**, *597*, 445-463